Chemical Engineering Science 120 (2014) 149–166

Contents lists available at ScienceDirect

Chemical Engineering Science

journal homepage: www.elsevier.com/locate/ces

Kinetics of the reduction of wüstite by hydrogen and carbon monoxide for the chemical looping production of hydrogen

Wen Liu [a,*], Jin Yang Lim [b], Marco A. Saucedo [a], Allan N. Hayhurst [b], Stuart A. Scott [a], J.S. Dennis [b]

[a] Department of Engineering, University of Cambridge, Trumpington Street, Cambridge CB2 1PZ, United Kingdom
[b] Department of Chemical Engineering and Biotechnology, University of Cambridge, Pembroke Street, Cambridge CB2 3RA, United Kingdom

HIGHLIGHTS

- Kinetics of the reduction of porous particles of wüstite by H_2 and CO were studied using fluidised beds.
- The intrinsic rates are the first order with respect to the concentration driving force in the gas phase.
- Activation energies for the rate constants were estimated.
- The reduction was found to undergo three different stages.
- Models and rate expressions were proposed to describe the intrinsic kinetics.

ARTICLE INFO

Article history:
Received 21 March 2014
Received in revised form
11 July 2014
Accepted 6 August 2014
Available online 13 August 2014

Keywords:
Kinetics
Chemical looping
Carbon capture
Hydrogen

ABSTRACT

Hydrogen of very high purity can be produced *via* the steam-iron process, in which steam oxidises metallic Fe in $3/4Fe+H_2O \rightarrow 1/4Fe_3O_4+H_2$. It is then advantageous to oxidise Fe_3O_4 in air to Fe_2O_3, an oxygen-carrier. This higher oxide of Fe is then reduced to regenerate metallic iron by reacting with synthesis gas, producing metallic Fe and possibly some wüstite (Fe_xO, $0<x<1$). In this three-stage process, the reduction of Fe_xO to Fe is the slowest reaction. This paper is concerned with the kinetics of the reduction of wüstite (Fe_xO) by reaction with CO, and, or H_2. Starting with pure (99 wt%) wüstite, the intrinsic kinetics of its reduction to metallic iron were measured in fluidised beds at different temperatures. The reaction was found to have 3 distinct stages, (i) the removal of lattice oxygen in wüstite, (ii) rate increasing with conversion of solid and (iii) rate decreasing with conversion of solid. A random pore model was used to simulate the latter stages of the reduction of wüstite by either H_2 or CO or a mixture of the two. It was found that the intrinsic rate of reduction in H_2 is substantially faster than with CO, whereas the resistances to diffusion of H_2 and CO through the product layer of Fe are comparable; these factors account for differences in the overall rates observed with these gases.

1. Introduction

Hydrogen is an environmentally-benign energy vector, since the combustion of hydrogen produces water as the sole product. However, to fuel a hydrogen economy, hydrogen would probably need to be generated by the consumption of another energy source, such as a carbonaceous fuel, e.g. from methane by reforming with steam, followed by the water-gas shift reaction. A significant contaminant of the hydrogen produced from reforming is CO, which restricts the use of the hydrogen in proton exchange membrane fuel cells, in which the Pt anodes are poisoned by CO with a volume fraction as low as 5×10^{-5} (Choudhary and Goodman, 2002). Alternatively, pure hydrogen can be produced by reacting steam with iron at high temperatures in the steam-iron process (Messerschmitt, 1910), employing:

$$3/4Fe+H_2O \rightleftarrows 1/4Fe_3O_4+H_2 \quad \Delta H^{o}_{1123\ K}=-26.3\ kJ/mol \qquad (1)$$

Reed and Berg (1953) proposed three inter-connected fluidised beds to run the steam-iron process continuously, by successively reducing and oxidising iron oxides using:

$$3Fe_2O_3+H_2 \rightleftarrows 2Fe_3O_4+H_2O, \quad \Delta Ho1123\ K=-5.9\ kJ/mol \qquad (2)$$

Abbreviations: b.c.c, body-centred cubic; BET, theory of Brunauer: Emmett and Teller; CCS, carbon capture storage; CSTR, continuous stirred tank reactor; I.D, internal diameter; PEMFC, proton exchange membrane fuel cell; PFR, plug flow reactor; SEM, scanning electron microscopy

* Corresponding author.
E-mail address: wl247@cam.ac.uk (W. Liu).

http://dx.doi.org/10.1016/j.ces.2014.08.010

$$\frac{x}{4x-3}Fe_3O_4 + H_2 \rightleftarrows \frac{3}{4x-3}Fe_xO + H_2O, \quad \Delta H^o{}_{1123K} = +56.6\ \text{kJ/mol} \tag{3}$$

$$Fe_xO + H_2 \rightleftarrows xFe + H_2O, \quad \Delta H^o{}_{1123K} = -16.9\ \text{kJ/mol} \tag{4}$$

$$3Fe_2O_3 + CO \rightleftarrows 2Fe_3O_4 + CO_2, \quad \Delta H^o{}_{1123\ K} = -40.8\ \text{kJ/mol} \tag{5}$$

$$\frac{x}{4x-3}Fe_3O_4 + CO \rightleftarrows \frac{3}{4x-3}Fe_xO + CO_2, \quad \Delta H^o{}_{1123\ K} = +34.9\ \text{kJ/mol} \tag{6}$$

$$Fe_xO + CO \rightleftarrows xFe + CO_2, \quad \Delta H^o{}_{1123\ K} = -16.6\ \text{kJ/mol} \tag{7}$$

$$2Fe_3O_4 + 1/2O_2 \rightleftarrows 3Fe_2O_3. \quad \Delta H^o{}_{1123\ K} = -237.2\ \text{kJ/mol} \tag{8}$$

Here Fe_xO represents the oxide of Fe(II), *viz.* wüstite, which contains metal-deficient sites in its crystalline lattice, so that the ratio of Fe to O is variable within limits (Giddings and Gordon, 1973), discussed below. The first step in the above process is the reduction of Fe_2O_3 (haematite), a so-called "oxygen-carrier", to a mixture of wüstite and Fe by synthesis gas; this occurs in reactions (2)–(4) with H_2 and (5) – (7), when the gaseous reductant is CO. Reducing almost 100% of the oxygen-carrier to metallic Fe is undesirable, because iron then catalyses the Boudouard reaction, causing the oxygen-carrier to coke. The result is that the hydrogen produced from the subsequent oxidation of the reduced carrier to Fe_3O_4 (magnetite) by steam (*i.e.* the reverse reactions of (3) and (4)) will be contaminated with CO. In the final step, Fe_3O_4 is oxidised in air to Fe_2O_3 in reaction (8), which supplies a considerable amount of heat for use within the plant or for export. Accordingly, the reduction of Fe_2O_3 by synthesis gas, the oxidation of Fe_xO and metallic Fe by steam and the oxidation of Fe_3O_4 in air are undertaken in the "fuel reactor", "steam reactor" and "air reactor", respectively. This can be achieved by either (i) having three different operating conditions in a single reactor, *e.g.* a packed bed with concentration gradients (Bohn et al., 2008), or (ii) three interconnected fluidised beds, allowing oxygen-carriers to circulate between them. Ideally, with an optimised design, the gaseous products leaving the fuel reactor will contain only CO_2 and H_2O. After condensation of steam, the CO_2 produced could be stored, *e.g.* by geological sequestration, making the overall process "carbon-neutral", or "carbon-negative" when biomass is used as fuel. In addition, the hydrogen produced during the oxidation of Fe_xO and metallic Fe in steam can be kept free from contaminants such as CO, provided coking does not occur; this avoids additional steps purifying hydrogen.

To completely convert the fuel to H_2O and CO_2 in the fuel reactor, the solid at the exit of the gas stream must be an equilibrium mixture of magnetite and haematite (Cleeton et al., 2009) at *e.g.* 1123 K. Therefore, a fluidised bed cannot be used as the fuel reactor for this process. Li et al. (2010) have proposed an improved design, which replaces fluidised beds with moving beds for both the reduction of Fe_2O_3 and the oxidation in steam to minimise axial mixing and allow the conversion of Fe_2O_3 to Fe to reach up to 50 %, (giving 46% of the stoichiometric yield of hydrogen after oxidising the reduced bed using steam), while maintaining effectively 100% conversion of H_2 and CO to H_2O and CO_2 at the exit of the fuel reactor. Alternatively, Bohn et al. (2008) proposed using a fixed bed to run the cyclic reactions in a semi-continuous fashion, allowing some iron oxide to be reduced to a stage where it can be used for producing H_2, whilst maintaining effectively 100% conversion of fuel at the outlet of the "fuel reactor".

Since the intrinsic rate of reduction of Fe_2O_3 by syngas is much slower than the rate of oxidation of the reduced oxides, or metal, by steam or air, the residence time of the oxygen-carriers in the fuel reactor (*i.e.* where their reduction takes place) is the longest. This sets constraints on parameters such as the circulation rate and the overall inventory of carrier particles, when designing a system of continuous fluidised beds. Similarly, in a system of fixed or moving beds, slow kinetics leads to low utilisation of the beds. As noted above, iron oxide undergoes three phase transitions during reduction, of which the slowest is the reduction of wüstite to iron (Liu et al., 2012a). However, the oxidation of Fe by steam produces about four times as much hydrogen as the oxidation of wüstite by steam, so that reducing the iron oxide fully to metallic iron is important for achieving the maximum yield of hydrogen per unit mass of oxygen-carrier.

There have been extensive studies of the reduction of wüstite in the fields of metallurgy and metal corrosion. Experimental work has mainly focused on two extreme cases: (i) the reduction of finely-powdered wüstite (Coombs and Munir, 1990; Mondal et al., 2004; Ryzhonkov and Sorin, 1999) and (ii) the reduction of dense slabs of wüstite of millimetre thickness (Hayes, 1979; John and Hayes, 1982; John et al., 1984; Turkdogan and Vinters, 1972). In both cases, the intrinsic rates of reaction are generally considered to be first order with respect to the chemical driving force in the gas phase, being $\{[CO]-[CO_2]/K_{p7}\}$ for reaction (7), where K_{p7} is its equilibrium constant, equal to the ratio of $[CO_2]$ to [CO] in the gas phase in equilibrium with the solid reactant and product. Typically, when the overall rate is controlled by intrinsic chemical reaction, the specific rate of reaction per unit mass of solid reactant can be expressed as:

$$r' = \frac{1}{\rho_{Solid}} \times A' \exp\left(-\frac{E}{RT}\right) \times \text{chemical driving force in gas phase} \times f(X) \tag{9}$$

Here ρ_{Solid} is the mass density of the solid reactant; A' is a pre-exponential factor for the intrinsic rate constant; $k_i = A' \exp(-E/RT)$; E is the activation energy and X is the fractional conversion of the initial oxide. For fine powders, the rate is often considered to be the first order with respect to the fraction of solid reactant present, so that in Eq. (9) $f(X) = (1-X)$ (Ryzhonkov and Sorin, 1999).

Where the reduction of dense slabs of wüstite has been measured, it has been generally found that the reduction can be divided into three stages with different time-scales, namely (i) a reduction of the stoichiometric ratio of O:Fe prior to the nucleation of iron (John et al., 1984), (ii) nucleation and growth of iron on the surface of the solid (Moujahid and Rist, 1988), and (iii) a slow growth of layers of Fe as product (John and Hayes, 1982). These layers of Fe affect significantly the diffusion of oxygen ions from the underlying wüstite to the outer surface of the Fe, where they react with gaseous reductant (Farren et al., 1990).

For chemical looping applications, oxygen-carriers are usually sub-millimetre porous particles, composed of sub-micron solid grains. They are thus different from the particles mentioned in the above studies. Accordingly, the aim of this research was to measure the rate of reduction of unsupported wüstite by hydrogen and also carbon monoxide in reactions (4) and (7), and to derive their rate expressions and kinetic parameters. Of course, in a practical chemical looping process, one would never perform reactions (4) and (7) on pure, unsupported wüstite, but instead, it would be supported on a ceramic oxide, such as alumina or zirconia. This is because pure wüstite sinters, particularly when reduced to Fe metal, giving a substantial fall in reactivity after a single redox cycle. In fact, stable reactivity of wüstite can be usually achieved by supporting it on *e.g.* Al_2O_3 (Kierzkowska et al., 2010) or ZrO_2 (Liu et al., 2012a). Nevertheless, by studying the kinetics of unsupported wüstite, the complicating effects of supporting materials on the kinetics can be excluded.

2. Experimental

2.1. Materials preparation

The method of wet-granulation (Bohn et al., 2008) was used to prepare "unsupported" particles of haematite (Fe_2O_3). Typically, granules of haematite were formed by spraying deionised water on to dry, powdered haematite of $d_p \approx 0.5$ μm (99 wt%, Sigma-Aldrich). The granules were sieved to the desired size fraction (*viz.* d_p=300–425 μm or 150–212 μm), roasted in air at 1223 K for ~3 h and after cooling were sieved again. Particles of wüstite were prepared by reducing 20.0 g of granulated haematite particles in a fluidised bed (described below in Section 2.2) containing only particles of Fe_2O_3, fluidised by an equimolar mixture of CO_2 and CO in N_2 at 1073 K, with $y_{CO} \approx 0.085$. The total flowrate of fluidising gas was 2.85 L min^{-1} (measured at 295 K, 1 atm). Under such conditions, the thermodynamically-stable phase of iron oxide is wüstite, with a stoichiometry of $Fe_{0.933}O$, according to Giddings and Gordon (1973) correlation. To confirm the complete conversion of Fe_2O_3 to wüstite, the concentrations of CO_2 and CO in the off-gas were measured with time; when the gas composition in the outlet matched that of the inlet, the reduction was assumed to be complete. Analysis of the gas concentration profiles also confirmed that the conversion to wüstite was complete, *i.e.* when:

$$X_{Wüs} = \frac{\dot{N}_{tot}}{5.31 \times 10^3 \times m_{Fe_2O_3}} \int_0^{t_\infty} (y_{CO_2,outlet} - y_{CO_2,inlet})\, dt = 1.0 \quad (10)$$

Here $\dot{N}_{tot}$ is the total molar flowrate of the inlet gas in mol s^{-1}, $m_{Fe_2O_3}$ the total initial mass in g of Fe_2O_3, t_∞ the total time of reduction in s and $y_{CO_2,inlet}$ and $y_{CO_2,outlet}$ the mole fractions of CO_2 at the bed's inlet and outlet, respectively. The constant 5.31×10^{-3} mol g^{-1} is the stoichiometric number of moles of CO_2 produced per g of Fe_2O_3 during the reduction to $Fe_{0.933}O$, as described above. The wüstite particles recovered from the bed were sieved again to ensure that only those in the size range, d_p=300–425 μm, were used in subsequent experiments.

2.2. Fluidised bed experiments

The kinetics of the reduction of wüstite were measured in a fluidised bed of white alumina sand (d_p=425–500 μm); the tubular reactor (i.d. 20 mm) has been described by Liu et al. (2012a) and was made of recrystallised α-Al_2O_3 (99.7%, Multi-lab Ltd.). The fluidising gases were taken from cylinders of: (i) N_2 (Air Liquide UK), (ii) 4.9 vol% H_2 in N_2 (BOC Ltd.), (iii) CO_2 (Air Liquide UK) and (iv) 9.5 vol% CO in N_2 (BOC. Ltd). A total flowrate of gas of ~2.5 L/min (measured at 295 K, 1 atm) was always fed to the electrically-heated fluidised bed. At this flowrate, assuming the bed of alumina sand was fluidised solely by N_2, U/U_{mf} was 3.3 at 923 K and 4.8 at 1173 K, where U is the superficial gas velocity and U_{mf} is the minimum fluidisation velocity, calculated according to Wen and Yu (1966) correlation. All this means that the bed was a bubbling one with an expanded depth of ~50 mm and a mean residence time of gas in the bed of ~0.1 s. Measurements were made only when the temperature of the bed was steady, which normally took ~40 min from a cold startup. The off-gas from the fluidised bed was sampled at a flowrate of ~1.0 L/min (measured at 295 K, 1 atm) using a quartz sampling probe above the fluidised bed and a diaphragm pump. The mole fractions of CO, CO_2 and H_2 were measured by two types of gas analyser, *viz.* a non-dispersive infrared analyser for CO and CO_2 (Uras 26, EL3020, ABB Ltd., 90% response time of 2.5 s under gas flow of 1 L min^{-1}) and a thermal conductivity analyser for H_2 (Caldos 27, EL3020, ABB Ltd., 90% response time of 2 s under a gas flow of 1 L min^{-1}).

The concentration profiles of the gaseous species H_2, CO and CO_2, were deconvoluted by assuming that the passage of a sample of gas from the fluidised bed through the sampling train could be described by one continuously stirred tank reactor (with a mean residence time, τ_M), connected in series with a plug flow reactor (residence time t_d). The values of τ_M and t_d were determined for this system by introducing step changes to the gas concentrations in the inlet, while measuring the dynamic response in the outlet. In this case, the corrected concentration C_C, was computed from $C_C = C_M + \tau_M dC_M/dt$, where C_M is the measured concentration (after smoothing using the Savitzky–Golay filter with a degree of 3 and a spam of 5 points), with dC_M/dt calculated using the same Savitzky–Golay filter. When a single gas analyser was connected, the mixing times, τ_M for the gas analysis train, *i.e.* the sampling lines plus the gas analysers, were found to be ~1.0 s and 1.5 s for H_2 and CO_2+CO analysers, respectively; when both analysers were connected in parallel; $\tau_M \approx 1.5$ s for both analysers.

In a typical experiment to measure their rates of reaction, a small weighed batch of wüstite particles was dropped into the bed of hot sand, when fluidised by a reducing gas mixture of H_2 or CO in N_2. After reduction, when the concentration of CO or H_2 in the off-gas had returned to that in the fluidising gas, a new batch of wüstite particles was added for a repeat experiment. Whenever the rate of reaction was sufficiently fast, the overall rate could have been governed by heat or mass transfer, instead of the intrinsic kinetics. To explore the extent of these effects, preliminary experiments were performed using haematite (Fe_2O_3) particles, whose reduction is the fastest of the oxides of iron. These results are discussed in Section 3; they enabled conditions suitable for measuring the intrinsic kinetics for the reduction of wüstite to be selected.

2.3. Characterisation of solids

The structures of the solid samples were examined by scanning electron microscopy (SEM, JOEL 5800LV) and mercury-intrusion porosimetry. For SEM, the solid samples were sputter-coated by a thin layer (thickness < 100 nm) of gold, before being examined under a vacuum (< 1 mbar) with an accelerating voltage of 15 kV. The pore size distribution (for 0.20 mm > d_{pore} > 7 nm) of particles of Fe_2O_3 was measured by a mercury porosimeter (Micromeritic-sAutopore IV 9500) at 298 K.

3. Parameters affecting the measurement of kinetics

3.1. Preliminary study of reduction of haematite

First, a batch of Fe_2O_3 (d_p=300–425 μm) was dropped into a bed of alumina sand (d_p=425–500 μm) fluidised by 4.95 vol% H_2 in N_2, when the temperature was steady. The specific rate of reaction was calculated from the measured change in the mole fraction of H_2, using

$$r' = \frac{(y_{H_2,inlet} - y_{H_2,outlet})}{m_{Fe_2O3}} \times \dot{N}_{tot} \quad (11)$$

where m_{Fe_2O3} is the initial mass of haematite in the batch and $\dot{N}_{tot}$ is the total molar flowrate of fluidising gas.

The resulting r' is plotted in Fig. 1, where t=0 corresponds to just before a measured concentration changed. Fig. 1 shows a spurious maximum in the specific rate at t=3 s, because the system takes ~3 s to produce genuine measurements of r'. In fact, Bohn et al. (2010) found that the reduction of Fe_2O_3 has a very fast initial rate. Therefore the fact that the first rate peaked at t=3 s suggests that the initial "settling or response time" for the system is about 3 ± 1 s, during which period the added Fe_2O_3 is being mixed in the bed, whilst the composition of the gases in and above

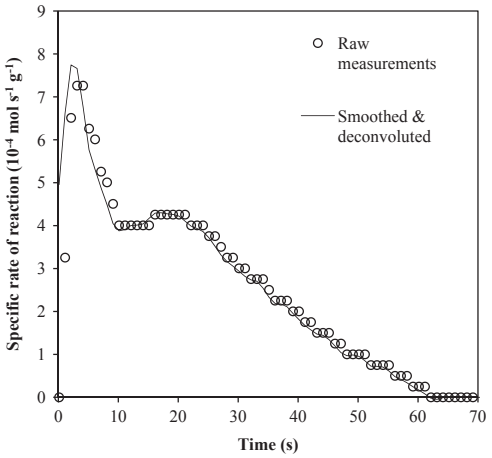

Fig. 1. The specific rates of reduction, derived from: (a) raw measurements and (b) measurements after smoothing and deconvolution, *versus* time, when a batch of 0.0260 g of granulated Fe_2O_3, sized to 300–425 μm, was added to a bed fluidised by 4.95 vol% H_2 in N_2 at 1223 K. The markers represent measurements taken at a frequency of 1 Hz.

the bed are changing rapidly. Therefore, in this study, with a sampling frequency of 1 Hz, the first 3 or 4 measurements after adding a batch of wüstite, should probably be disregarded.

Subsequently there is a fall to a local minimum at $t=11$ s; then a second maximum is followed by a steady decline, reaching zero at ~62 s; this profile is typical for the reduction of Fe_2O_3. Based on a balance on oxygen, it is found that the minimum at $t=11$ s corresponds to a point where Fe_2O_3 is reduced fully to wüstite. Therefore, the initial rate can be identified as involving the reduction of Fe_2O_3 to Fe_3O_4 and subsequently to wüstite, whereas at the second maximum there is the reduction of wüstite to Fe. It seems that under the current conditions, the reductions from Fe_2O_3 to Fe_3O_4 and then to wüstite are both fast, and cannot be distinguished from the first peak in Fig. 1. There is also some overlap between the reduction of Fe_3O_4 to wüstite and wüstite to Fe, especially around the local minimum after 11 s. A comparison of the two maxima indicates that the rate of reduction of wüstite is slower than the preceding steps.

In general, deconvolution was most needed when the rate of reaction was fastest, *e.g.* at early times when a batch of haematite (Fe_2O_3) was reduced in hydrogen at 1173 K, as shown in Fig. 1. The result after data smoothing and deconvolution (with $\tau_M=1$ s) for this case is compared in Fig. 1 with the raw results without deconvolution. Fig. 1 suggests that, for $t>4$ s, mixing in the sampling system did not alter the original concentration profile significantly. However, for the subsequent slow reaction between H_2 and CO and wüstite, the measured concentration profiles for $t>3$ s were used without deconvolution, because of Fig. 1.

3.2. Effect of heat transfer between the fluidised bed and a particle

The heat balance in the steady state on a reacting, porous, spherical particle of wüstite, radius R_0, gives:

$$r'\Delta H_T^{\circ}\rho_{FeO}\left(\frac{4\pi {R_0}^3}{3}\right)=h(4\pi {R_0}^2)(T-T_\infty), \tag{12}$$

where ΔH_T° is approximated by $\Delta H_{T_\infty}^{\circ}$, the heat of reaction (4) at T_∞, the temperature of the bed, estimated using Barin's thermodynamic database (1973), assuming ΔH_T° varies very little over the temperature range of concern; T is the temperature of the particle and h is the overall heat transfer coefficient between the particle and the bed. Bohn et al. (2010) assumed $h\approx 300$ W m^{-2} K^{-1}, corresponding to Nu=2. If the rate of reduction of wüstite to Fe is 4×10^{-4} mol s^{-1} g^{-1} (*viz.* the second maximum in Fig. 1), Eq. (12) indicates that the temperature difference between a particle's ($R_0=180$ μm) exterior and the bed is $(T-T_\infty)\sim3$ K, *i.e.* negligible.

3.3. Effect of interphase mass transfer

The resistance to mass transfer of a gaseous reactant from the bubble to the particulate phase is potentially important. Had there been a substantial resistance to such interphase mass transfer, the measured composition of the off-gases would have differed from that in the particulate phase, thereby "blurring" the measurement of intrinsic kinetics. This is the case when the rate of reaction is much faster than the rate of interphase mass transfer. Accordingly, the cross flow factor (Davidson and Harrison, 1963) for the fluidised bed, $X_{fl}=QH/V_bU_b$, was estimated. Here $Q=3U_{mf}\pi d_b^2/4$ is the volumetric crossflow assuming mass transfer by molecular diffusion is negligible, H is the depth of the fluidised bed, V_b is the volume of a bubble, U_b is the rise velocity of a bubble and d_b is the effective diameter of a bubble. The arithmetic mean diameter of a bubble can be calculated using the correlation of Darton et al. (1977):

$$d_b=\frac{0.54(U-U_{mf})^{0.4}}{g^{0.2}H}\int_0^H(h-4\sqrt{A_0})^{0.8}\,dh, \tag{13}$$

where h is the vertical distance above the distributor and $A_0=7.85\times10^{-7}$ m^2 is the catchment area of the inlet stream. The correlations from Davidson and Harrison (1963) for bubble velocity and the bed's expansion:

$$U_b=0.711\sqrt{gd_b}, \tag{14}$$

$$\frac{H-H_{mf}}{H_{mf}}=\frac{U-U_{mf}}{U_b}, \tag{15}$$

were also used to calculate U_b and H. Here H_{mf} is the depth of the fluidised bed at incipient fluidisation. To calculate H and d_b, Eqs. (13)–(15) were solved simultaneously; the resulting values of X_{fl} are in the range between 7.0 (at 923 K) and 5.3 (at 1123 K). It should be noted that, the exclusion of a molecular diffusion term in the expression of Q means underestimated values of X_{fl}. Nevertheless, these underestimated values of X_{fl} are already large enough (>2.5) for the gas in the particulate and bubble phases to be well-mixed, *i.e.* there was insignificant resistance to interphase mass transfer for the temperature range used.

To determine experimentally the operating regime in which interphase mass transfer is unimportant, different masses of haematite (Fe_2O_3) were reduced by H_2 in the fluidised bed at 1073 K. Fig. 2 shows the apparent specific rates falling, for the reduction of Fe_2O_3 to wüstite (the first fall in rate in Fig. 2) and the subsequent reduction to Fe (the second drop). These plots are independent of the mass of the added Fe_2O_3, provided this was less than 0.04 g; this reveals the condition for interphase mass transfer to be unimportant. Since intrinsic kinetics are much more sensitive to temperature than mass transfer, the maximum mass of a batch was reduced accordingly to compensate for the faster intrinsic kinetics at higher temperatures. Based on the value of $E=69$ kJ mol^{-1} from the review by Hayes (1979), the maximum mass of solid reactant was thus varied according to $1/m_{FeO}\propto\exp(-E/RT)$.

3.4. Effect of external mass transfer

External mass transfer in this context refers to that from the gas in the particulate phase to the external surface of a reacting particle of wüstite. The Sherwood number is given (Dennis and Hayhurst, 1986) by: $Sh=2\varepsilon_{mf}+0.6Re^{0.8}Sc^{0.6}=k_gd_p/d_M$. Here $Re=2.5\,U_{mf}\,d_p\,/\varepsilon_{mf}\,\upsilon$. Calculations were undertaken for the most

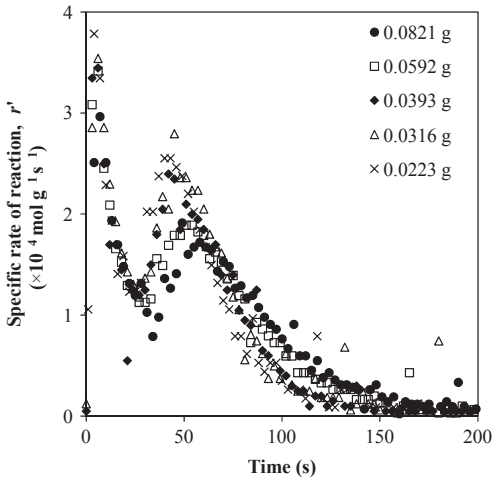

Fig. 2. Specific rates of reduction as functions of time, when different batches of Fe_2O_3 were added to a bed, fluidised by 4.95 mol% H_2 in N_2 at 1073 K. The time interval between consecutive points is 3 s.

extreme cases, when the rate of chemical reaction was the fastest, *i.e.* the reduction of Fe_2O_3 in H_2 at 1173 K. At these conditions, $U_{mf}=0.07\ m\ s^{-1}$, the voidage in the particulate phase at minimum fluidisation, $\varepsilon_{mf}\approx 0.42$, the diameter of an iron oxide particle $d_p=3.6\times10^{-4}$ m, the kinematic viscosity of the gas $\upsilon=1.57\times10^{-4}\ m^2\ s^{-1}$ (from Sutherland's (1893) formula), and $Sc=\upsilon/D_M$, with $D_M=7.5\times10^{-4}\ m^2\ s^{-1}$ being the molecular diffusivity of H_2 in N_2, calculated using the Chapman–Enskog formula (Green and Perry, 2007). Thus, the coefficient of mass transfer, $k_g=2.2\ m\ s^{-1}$, which corresponds to a maximum specific rate of mass transfer of $7.7\times10^{-3}\ mol\ g^{-1}\ s^{-1}$, when the mole fraction of the reducing gas, H_2, is 4.95 mol%. Of course, when H_2 is the reactant in reaction (4), the condition of equimolar counter-diffusion is satisfied. This estimated maximum rate of external mass transfer is one order of magnitude faster than the highest observed overall rate in Fig. 1. Hence it may be concluded that external mass transfer was also insignificant when wüstite is being reduced.

3.5. *Effect of accumulation of reacted particles*

Several measurements were performed using the same fluidised bed, by dropping five consecutive batches of haematite into the hot bed fluidised by 2.5 L min^{-1} (measured at 295 K, 1 atm) of 10 vol% CO in N_2. Each addition was made after the previous batch had been fully reduced to Fe. It was found that the apparent rate profiles of all five batches were almost identical, suggesting that the accumulation of relatively small amount of iron did not affect the measurements.

4. Results for the reduction of wüstite

4.1. *Analysis of experimental results*

Typical profiles of the mole fractions of H_2 and both CO and CO_2 in the off-gas after adding a batch of wüstite particles to a bed fluidised, respectively, by H_2 and then CO in N_2, are shown in Fig. 3. Particularly with reduction by CO, the raw measurements in Fig. 3 appear in steps. This was because of the low sensitivity of the data acquisition system, which was limited by the resolution of the data card and the gas analysers. For example, changes in mole fractions of CO and CO_2 of less than 0.04 vol% could not be measured directly. Also, as discussed above, to minimise the effects of heat and mass transfer, the overall rate of reaction was intentionally kept low. Consequently, the resolution of the raw

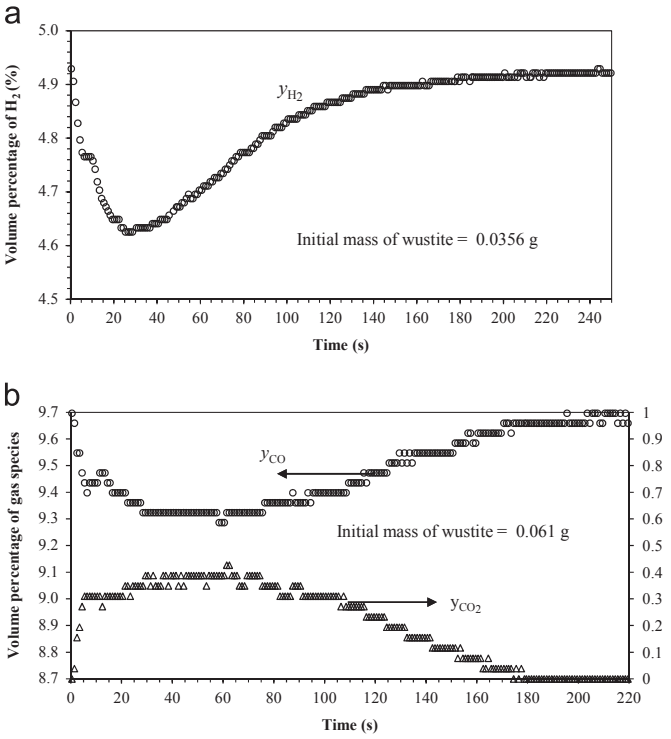

Fig. 3. Volume percentage of gaseous species *versus* time, as measured the off-gas, when a small batch of particles of wüstite (size fraction 300–425 μm) was added to a bed of alumina sand (size fraction 425–500 μm) fluidised by (a) 4.95 vol% H_2 in N_2 or (b) 9.7 vol% CO in N_2, at 1123 K in 1 atm pressure. The time-interval between consecutive points is 1 s.

measurements was limited, leading to the appearance of step changes in Fig. 3. This limited resolution, *i.e.* the low signal-to-noise ratio in the raw measurements is the dominating source of random error in these experiments. Consequently, all specific rates were measured using an equation analogous to (11), in which m_{Fe2O3} was replaced by m_{FeO} and y_{CO2} was used when CO was the reactant; their errors were the signal-to-noise ratios of the raw measurements. To approximate the continuous profiles of concentrations, the raw measurements were smoothed by a moving average algorithm with a variable span equal to the mean number of measurements before and after the "step change", when measurements were taken at a frequency of 1 Hz.

Looking first at Fig. 3 (a), it can be seen that the initial rate is increasing during the first 3–4 s, when the bed is still "settling". A "point of inflection" then follows, with the rate steady at $t\sim7$–9 s; afterwards the rate rises to a maximum at ~25 s. Finally, the rate decreased slowly and reached zero after ~220 s. Thus there appear to be three phases for the reduction of wüstite in H_2: an initial period with what could be a constant rate, then one where the rate is increasing (accelerating) and a final stage, when the rate falls with increasing time. When wüstite was reduced in CO, similar features were seen in Fig. 3 (b) for the profiles of [CO] in the off-gas. In this case, a small peak was observed at ~6 s, followed by an apparent local minimum at $t\sim11$ s, and then a rise to a maximum between 50 and 60 s, before falling to zero, when $t\sim200$ s. Thus with CO as reactant, the initial stage with maybe a constant rate is not as conspicuous as with H_2. The profile of [CO_2] seems to reflect that of [CO], except for the absence of the small peak at $t\sim6$ s, because of the lower resolution of the raw measurements of y_{CO2}.

The conversions of wüstite ($Fe_{0.933}O$) to metallic Fe, were also calculated using:

$$X_{H_2}(t)=\frac{1}{0.01469}\frac{\dot{N}_{tot}}{m_{FeO}}\times\int_0^t[y_{H_2,inlet}-y_{H_2,outlet}(\tau)]\,d\tau, \qquad (16)$$

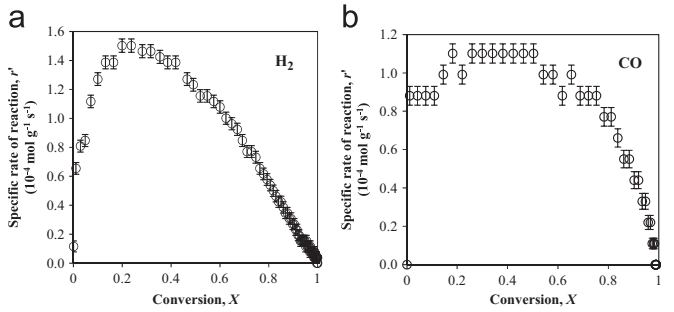

Fig. 4. Plots of specific rate of reduction *versus* conversion, for a small batch of particles of wüstite (size fraction 300–425 μm) added to a bed of alumina sand (size fraction 425–500 μm) fluidised by (a) 4.95 vol% H_2 in N_2 or (b) 9.7 vol% CO in N_2, at 1123 K in 1 atm pressure. The lines represent smoothed profiles; the points represent unsmoothed results. The error bars correspond to errors in individual measurements due to limits of detection of the gas analysers. For clarity, not all unsmoothed results are shown: one in three and one in five measurements are plotted for (a) and (b), respectively.

$$X_{CO}(t) = \frac{1}{0.01469}\frac{\dot{N}_{tot}}{m_{FeO}} \times \int_0^t y_{CO_2,outlet}(\tau)\, d\tau, \tag{17}$$

where m_{FeO} is the initial mass of wüstite particles in a batch and 0.01469 mol g^{-1} is the number of oxygen atoms per g of wüstite, as prepared in Section 2.1. Each experiment was repeated at least once to ensure reliability of the measurements.

By plotting the smoothed profiles of r' against X in Fig. 4, the relationship between rate and conversion can be examined. From Fig. 4, it appears that the initial rises in rate with both reactants take place, when $0 < X < 0.015$, followed by the "point of inflection", when $0.015 < X < 0.05$. The maxima in rate are at $X \sim 0.2$ and $X \sim 0.3$ for the reduction in H_2 and CO, respectively. During the third "decaying phase" at large conversions, the rate of reduction in the reactant, H_2, decreases almost linearly with conversion, whereas the plot in Fig. 4(b) with CO shows more curvature.

It is important to check whether there is any effect of intra-particle mass transfer on the measurements. For the reduction of haematite (Fe_2O_3) to magnetite (Fe_3O_4), and magnetite to wüstite, Bohn et al. (2010b) using similar apparatus and also particles of Fe_2O_3 and Fe_3O_4 prepared by very similar methods, demonstrated that the effectiveness factor, η was close to unity, when the particle's radius $R_0 \leq 180$ μm. For the reduction from wüstite to Fe, the chemical rate is much slower, so intra-particle diffusional resistance should be less significant, giving η closer to unity. To verify this assertion, wüstite particles sieved to two different sizes (150–212 μm and 300–425 μm) were separately reduced in either H_2 or CO, between 923 and 1223 K. Assuming first-order kinetics, the apparent rate constants, k_a, at iso-conversion points of $X=0.3$, where the rates for both reactions are near their maximum values in Fig. 3, were derived using

$$k_a(X) = (\text{specific rate of reaction})/(\text{concentration driving force}) \tag{18}$$

In equation (18), the concentration driving forces are ($[H_2]$–$[H_2O]/K_{p4}$) or ($[CO]$–$[CO_2]/K_{p7}$) with H_2 or CO as the respective reactants. Here K_{p4} and K_{p7} are, respectively, the equilibrium constants for reactions (4) and (7); the specific rate of reaction is given *e.g.* by equation (11). Arrhenius plots of the measured k_a for $X=0.3$ are shown in Fig. 5, which does not indicate that k_a is noticeably larger for small particles. Also, the gradients of these plots, *viz.* the apparent activation energies, are all 70 ± 10 kJ mol^{-1} and independent of particle size, suggesting that any resistance to intra-particle diffusion was insignificant. The values of the activation energies are discussed in more detail in Section 5.4. Consequently, the assumption that $\eta=1$ is experimentally confirmed, for all values of X, so the apparent rate constants can be treated as intrinsic rate constants. It is noteworthy that k_a is larger for H_2 than with CO as reactant.

4.2. Determining the intrinsic kinetics of reduction of wüstite by H_2

The order of reaction with respect to the chemical driving force, *i.e.* ($[H_2]$–$[H_2O]/K_{p1}$), was determined by plotting the measured specific rates of reaction against ($[H_2]$–$[H_2O]/K_{p1}$) at 1123 K. The specific rates at iso-conversion points of $X=0.05$, 0.1, 0.3 and 0.6 were derived using equation (11) and are plotted in Fig. 6. The good linearity with an intercept of zero confirms that the rate is indeed first order with respect to ($[H_2]$–$[H_2O]/K_{p1}$) for X between 0.05 and 0.6. The conversions of 0.05, 0.1, 0.3 and 0.6 were chosen, because they correspond to the stages of reaction, mentioned above. Thus, the specific rate of the reduction of wüstite by hydrogen can be expressed as:

$$r' = \frac{k_i}{\rho_{FeO}}\left([H_2] - \frac{[H_2O]}{K_{p4}}\right) f(X), \tag{19}$$

where $f(X)$ is a function describing the contribution by the conversion of solid, X, to the intrinsic kinetics - usually a feature determined by the structure of the solid reactant; k_i is the intrinsic rate constant (per unit volume of particle) in s^{-1}. The specific rate can be also expressed using k_A (in units of m s^{-1}), a rate constant

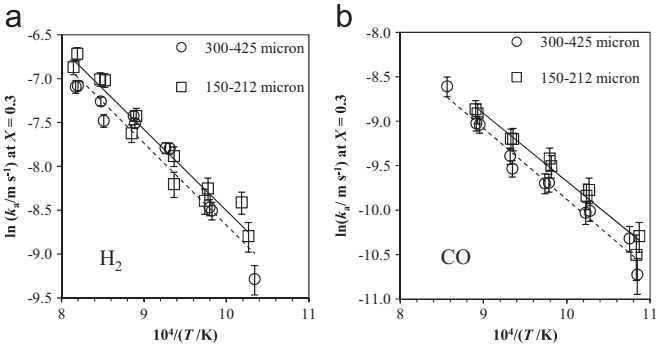

Fig. 5. Apparent rate constants at iso-conversions $X=0.3$ *versus* temperature using two different size fractions of wüstite particles, which were reduced in either H_2 in N_2 (left) or CO in N_2 (right) in a fluidised bed. The experimental errors correspond to errors in individual measurements due to limits of detection of the gas analysers.

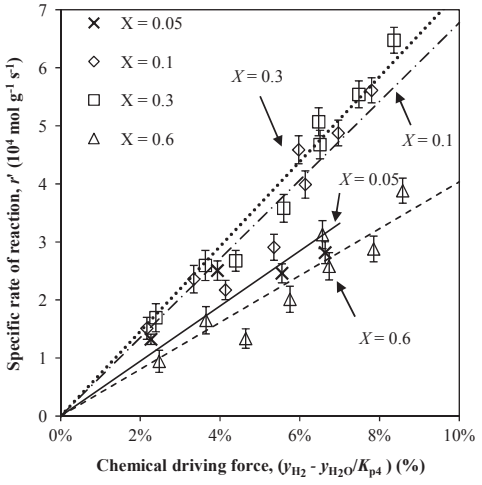

Fig. 6. The measured specific rates of reduction of wüstite *versus* ($[H_2]$–$[H_2O]/K_{p4}$) at iso-conversion points where $X=0.1$, 0.3 and 0.6, when a batch of wüstite particles was reduced by H_2 in N_2 at 1123 K in a fluidised bed. The concentration of H_2O was estimated from the deviation of the outlet $[H_2]$ from the inlet $[H_2]$. The error bars indicate errors in individual measurements due to limits of detection of the gas analysers.

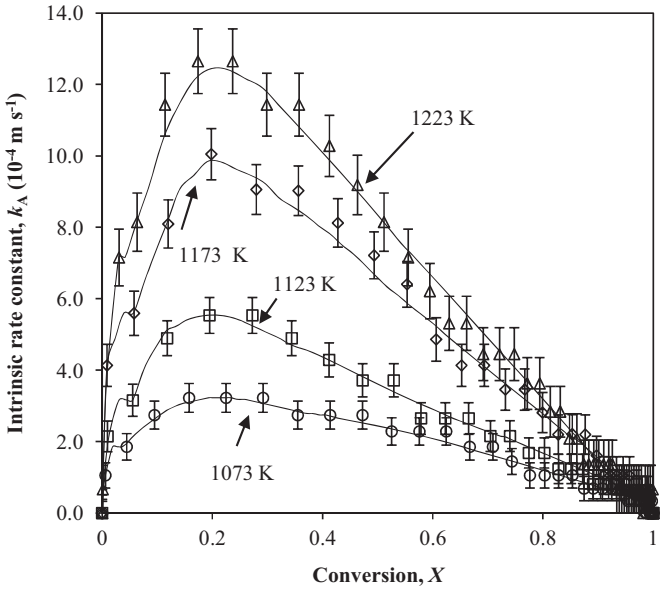

Fig. 7. The intrinsic rate constant k_A against conversion of wüstite (d_p=300–425 μm), calculated from the results of the reduction of wüstite in 4.95 vol% H_2 in N_2 at different temperatures. The lines represent the smoothed profiles, and the points represent measurements without smoothing. The error bars correspond to errors in individual measurements due to limits of detection of the gas analysers. For clarity, not all unsmoothed results are shown: one in every five, four, three and two measurements are plotted for 1073, 1123, 1173 and 1223 K, respectively.

based on the surface area of solid by:

$$r' = \frac{S_0 k_A}{\rho_{FeO}}\left([H_2] - \frac{[H_2O]}{K_{p4}}\right), \tag{20}$$

with $k_A = A\exp(-E/RT)$. Here S_0 is the specific surface area of the wüstite before reaction, A is the pre-exponential factor and E is the activation energy for k_A. Again, k_A is a function of the solid's conversion, X. Plots of the measured k_A versus conversion, X, at different temperatures are shown in Fig. 7 for H_2 as reactant.

Very interestingly, Fig. 7 suggests that, at all temperatures, the reaction is likely to be comprised of three phases, as described above in Section 4.1. In particular, the "point of inflection" at $X \sim 0.03$ is more obvious at lower than higher temperatures, because the reaction is slower at lower temperatures and more measurements were taken and not confused by the rapidly changing $[H_2]$ in the off-gas. The results at 1073–1223 K show consistently that with H_2, the rate has a maximum at $X \sim 0.2$; at $X > 0.2$ the rate declines and falls to zero when $X = 1$. The shape of the plotted curve of k_A against X is investigated in detail in Section 5.2.

The Arrhenius plots are shown in Fig. 8 for the initial phase at the points of inflections, where the rate was found to be constant. Using weighted linear regression, the lines of best fit indicate

$$k_A = 9.0\exp\left(\frac{96\text{kJ mol}^{-1}}{RT}\right) \text{m s}^{-1}, \tag{21}$$

during this initial phase. Here, the 95% confidence intervals of the fitted parameters gave 95% confidence bounds of 9.0 $(+11, -5)$ m s^{-1} and 96 ± 7 kJ mol^{-1} for A and E, respectively. The errors given for the kinetic parameters are derived from the 95% confidence intervals for the intercept and gradient of the Arrhenius plot. Aside from the usual qualification about the inherent assumptions in the weighted linear least squares analysis (*e.g.* normal distribution of errors with variance proportional to the weighting factors), as described by Barrie (2011), great care must be taken when quoting the errors in parameters from an Arrhenius

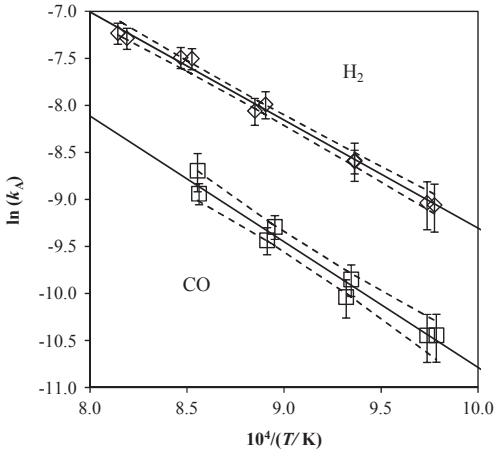

Fig. 8. Plot of ln(k_A) *versus* $1/T$ for the initial phase where the rate is constant, when small batches of wüstite (d_p=300–425 μm) were reduced by either 4.95 vol% H_2 in N_2 or 9.7 vol% CO in N_2, in a fluidised bed. Lines of best fit (using weighted least square linear regression) to both sets of results are also shown. The error bars correspond to errors in individual measurements due to limits of detection of the gas analysers. The dashed lines represent 95% confidence band for the fitted ln(k_A) (non-simultaneous functional band (MATLAB, 2008)).

plot, since the values of E and ln(A), and their errors are highly correlated. In this case the uncertainty in the fitting parameters ln (A) and E is best expressed by a confidence ellipse; for an Arrhenius plot, unless the temperature range used is unfeasibly large, the correlation between the parameters is so large this ellipse collapses almost to a line (Barrie, 2011). For a fixed activation energy, the error in ln(A) is small, but the overall uncertainty, without regard for the value of E, in ln(A) is large. The net result is that, the error given in E is the absolute uncertainty regardless of changes in other parameters, *i.e.* repeats of the experiment producing a large number of independent Arrhenius plots, would be expected to give gradients within the error bounds 95% of the time (*i.e.* despite the fact that the intercept, ln(A) would be varying in each plot). Here, the interest is mainly in the value of E alone, since this is often used to infer rate-controlling mechanisms, hence the error bound used is appropriate. Error bounds for absolute value of A are large because they are derived form a logarithm plot and do not account for the correlation with E, therefore it can be difficult to attach physical significance to the absolute value. The correlation between ln(A) and E means it is not appropriate to combine the error bounds for A and E and expect a reasonable estimate in the error in the rate constant. Accordingly, in the Arrhenius plots which follow (as in Fig. 8), confidence bands for the value of ln(k_A) are calculated, taking into account for the covariance between ln(A) and E.

To determine activation energies after the "constant rate period", the values of k_A were calculated at various iso-conversion points, *viz.* X=0.1, 0.3 and 0.6, and the resulting ln (k_A) are plotted against $1/T$ in Fig. 9, so that the contribution of X to k_A is kept constant and ignored at each iso-conversion point. Based on the gradient of the lines of best fit using weighted least squares linear regression, the activation energies were found to be 62 ± 9, 78 ± 11 and 79 ± 22 kJ mol^{-1} for X=0.1, 0.3 and 0.6, respectively, where the uncertainties are 95% confidence bands. The weighting factors were the inverse of the uncertainties in the y-values squared (Green and Margerison, 1978), so in the case of Fig. 9, $w_i = 1/[\Delta\ln(k_{Ai})]^2$, where w_i is the weighting factor for the ith point. Based on a statistical analysis of the measurements (an F-test, not shown here), the activation energy at X=0.1 differs from that at the two higher conversions with a confidence level of 93%, whereas the confidence level for E being the same at X=0.3 and X=0.6 is 91%. To rule out the possibility of the resistance from

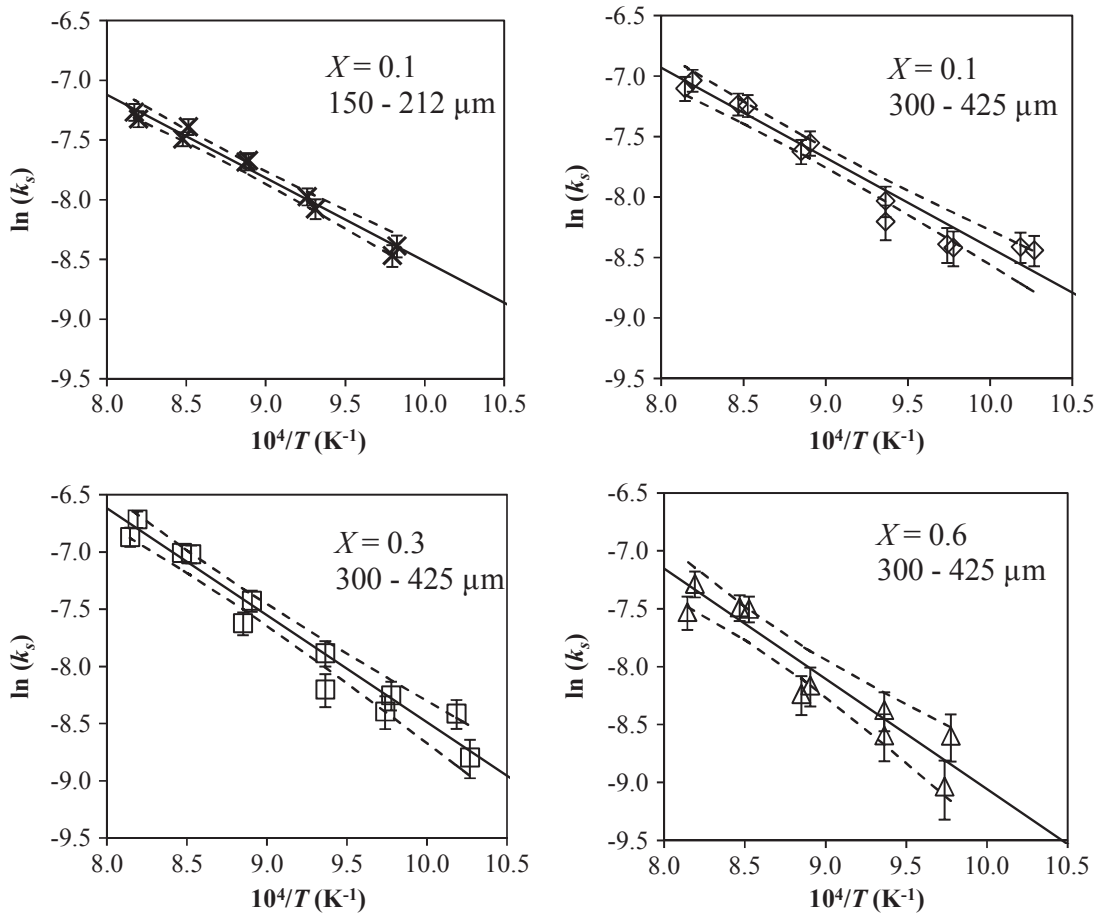

Fig. 9. Plots of $\ln(k_A)$ *versus* $1/T$ at iso-conversion points, when small batches of wüstite (d_p=300–425 μm) was reduced by 4.95 vol.% H_2 in N_2 in a fluidised bed. Results for for X=0.1, 0.3 and 0.6 for d_p=300–425 μm are shown, as well as results at X=0.1 using smaller wüstite particles (d_p=150–212 μm). Best linear fits (weighted least square linear regressions) at respective conversions are also shown. The error bars correspond to errors in individual measurements due to limits of detection of the gas analysers. The dashed lines represent 95% confidence band for the fitted $\ln(k_A)$ (non-simultaneous functional band (MATLAB, 2008)).

intra-particle diffusion lowering the apparent activation energy at X=0.1, the activation energy at X=0.1 was determined for particles of wüstite of half the size, *i.e.* sieve size fraction of 150–212 μm, as shown in Fig. 9. It was found that the activation energy for reduction of the smaller particles at X=0.1 is 58 ± 8 kJ mol^{-1}, *i.e.* similar to the value of 62 ± 9 kJ mol^{-1} for particles twice their size at the same conversion and very different from those measured at higher conversions (with 98% confidence). This suggests that the difference between the activation energies at low and high conversions is genuine and also that intra-particle mass transfer was not the cause of the lower activation energy. From the values of the activation energies derived above, it appears that the three phases seen in Figs. 4 (a) and 8 correspond to three different chemical processes. The shape of the profile of k_A in Fig. 7 shows that the transition between the accelerating phase and the decelerating phase is likely to take place at $X \approx 0.2$.

4.3. Determining the intrinsic kinetics of reduction of wüstite by CO

Analogous rate equations for the reduction of wüstite by the other reactant, CO, can be formulated, as:

$$r' = \frac{k_i}{\rho_{FeO}}\left([CO] - \frac{[CO_2]}{K_{p7}}\right) f(X), \tag{22}$$

$$r' = \frac{S_0 k_A}{\rho_{FeO}}\left([CO] - \frac{[CO_2]}{K_{p7}}\right), \tag{23}$$

where again the intrinsic rate constants, k_i and k_A, have an activation energy E. The specific rates of reaction, r', for CO reacting at iso-conversion points of X=0.05, 0.1, 0.3 and 0.6 are plotted in Fig. 10 against the chemical driving force, ([CO]–[CO_2]/K_{p7}). Fig. 10 shows that: (i) the rate is first order with respect to the concentration driving force, ([CO]–[CO_2]/K_{p7}), and (ii) unlike with H_2, the rate for CO is not a strong function of X, the conversion of the solid. For [CO] at the inlet kept constant, dX/dt is plotted against X in Fig. 11, which shows very small variations in rate at lower temperatures, for X increasing from 0.2 to 0.7.

Again, the plots in Fig. 11 suggest at least three phases of reaction, similar to reduction in hydrogen at 1123 K discussed above in Fig. 4. These phases are: (i) an initial peak at $0 < X < 0.05$, (ii) an increase in rate when $0.05 < X < 0.3$ and (iii) a decelerating phase, when $0.3 < X < 1$. In addition, a constant rate period is also conspicuous when $X \sim 0.05$, except for T=1173 K. The values of k_A derived for $X \sim 0.05$ are shown in Fig. 8. The line of best fit corresponds to:

$$k_A = \left(13\ ^{+105}_{-12}\right) \exp\left(\frac{111 \pm 20\ \text{kJ mol}^{-1}}{RT}\right) \text{m s}^{-1} \tag{24}$$

Here, the 95% confidence intervals of the fitted parameters gave 95% confidence bounds of 13 $(+105, -12)$ m s^{-1} and 111 ± 20 kJ mol^{-1} for A and E, respectively. Comparing the two plots in Fig. 8, it would seem that the chemical reaction when $X < 0.05$ for the reduction by CO is different from that by H_2, in spite of the similar values of E.

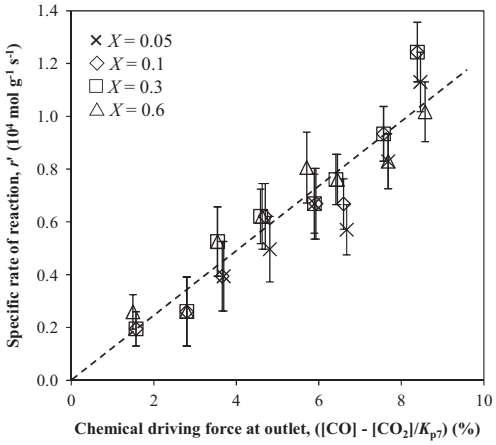

Fig. 10. The specific rates of reduction *versus* $(y_{CO}-y_{CO_2}/K_{p7})$ at iso-conversion points where X=0.1 (♦), 0.3 (■) and 0.6 (▲), when a batch of wüstite particles was reduced by CO of various mole fractions in N_2 at 1173 K in a fluidised bed.

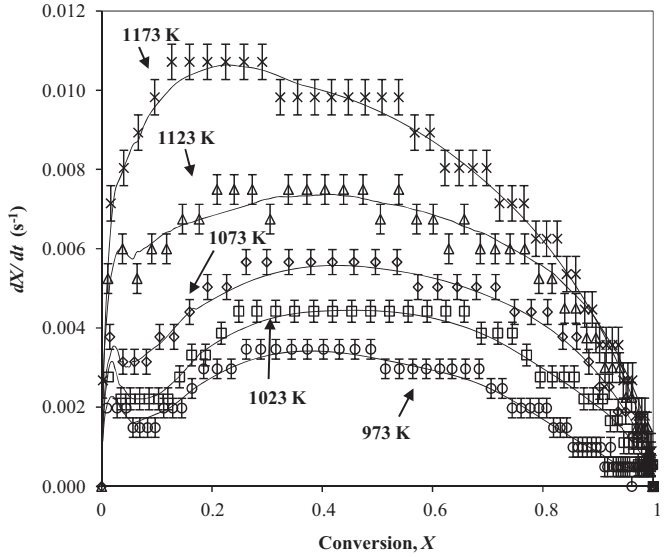

Fig. 11. The rate of conversion, dX/dt, plotted (in open symbols) against X, for the reduction of wüstite (d_p=300–425 μm) in 9.7 vol% CO in N_2 at different temperatures. The lines represent the smoothed profiles, and the points represent measurements without smoothing. The error bars correspond to errors in individual measurements. For clarity, not all unsmoothed results are shown: one in every seven, six, five, four and three measurements are plotted for 973, 1023, 1073, 1123 and 1173 K, respectively.

For $X > 0.05$, the plots are similar in shape in Fig. 11. There is a maximum rate at $X \sim 0.2$ at 1173 K, but at X between 0.3 and 0.4 at lower temperatures. At a given temperature, the values of k_A measured for the reduction in CO are about 1/3 of those measured for reduction in H_2. The Arrhenius plots for k_A at iso-conversion points of X=0.1, 0.3 and 0.6, are shown in Fig. 12. These plots were fitted with lines using a weighted least-square regression. The gradients of the lines of best fit gave activation energies of 83 ± 14, 71 ± 11 and 66 ± 15 kJ mol^{-1} for X=0.1, 0.3 and 0.6, respectively, where the values after $\pm$ indicate 95% confidence intervals. Here, the activation energy measured at X=0.1 is most likely to be different to those at X=0.3 and 0.6 with a confidence level of 76% (based on an F-test, not shown here), whereas the same activation energy measured at X=0.3 and 0.6 has a confidence levels of 62%. That the activation energy at X=0.1 exceeds those at higher conversions, rules out the possibility that the rate at low conversion (*e.g.* X=0.1) is controlled by intra-particle diffusion. Although the rate appears to be at a maximum at X=0.3 and decreasing at X=0.6,

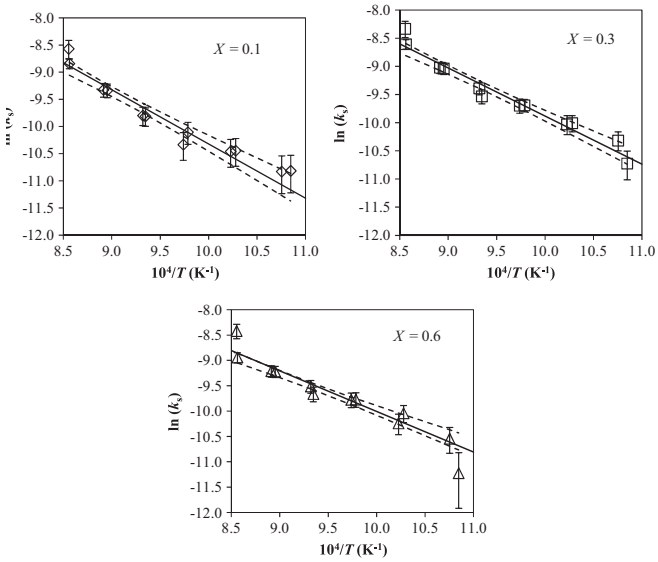

Fig. 12. Plots of $\ln(k_A)$ *versus* $1/T$ at different iso-conversion points, when a small batch of wüstite (d_p=300–425 μm) was reduced by 9.7 vol% CO in N_2 in a fluidised bed. Results at iso-conversion points X=0.1, 0.3 and 0.6 are analysed and plotted. Linear fits to the measurements at different X are also shown. The dashed lines represent 95% confidence band for the fitted $\ln(k_A)$ (non-simultaneous functional band (MATLAB, 2008)).

the similar activation energies for k_A measured at these two iso-conversion points suggest that the reactions at these two points are likely to be chemically identical, similar to the case for H_2. The values of A and E for k_A at three different conversions are tabulated and compared in Table 1. They are discussed in the next section.

5. Discussion

5.1. Introduction

Looking at Table 1, it is apparent that, at large X, the values of A for both H_2 and CO are different by an order of magnitude, meaning that the rate-determining step for the two reactions cannot be the same. Therefore, it is highly unlikely that, at high conversions, *e.g.* X=0.6, both reactions are controlled by diffusion of oxygen atoms through the product iron to some reaction zone at the interface between the solid and gas phases.

The values in Table 1 for A, the pre-exponential factor for k_A, should be compared with those for a reaction involving collisions of H_2 or CO with a solid surface. In that case, simple collision theory indicates:

$$A_{\text{theory}} = \frac{1}{4}\sqrt{\frac{8RT}{\pi M_i}}, \tag{25}$$

where M_i is the relative molecular mass of species i in kg kmol^{-1}. It should be noted that the temperature dependence of $T^{1/2}$ for the A factor is much weaker than that of k_A, so A is often assumed to be independent of temperature. Over the temperature range between 923 K and 1223 K, the values of A_{theory} calculated for H_2 and CO using Eq. (25) are 788–888 m s^{-1} and 227–247 m s^{-1}, respectively. In both cases, the measured values of A (though with the qualification that, as noted above, the error estimates for A are large) are at least two orders of magnitude smaller than those from collision theory. This means that mechanisms involving collisions of gaseous molecules with a solid surface cannot be ruled out.

Table 1
Comparison of pre-exponential factors and activation energies for k_A for the reduction of wüstite in H_2 or CO at iso-conversion points of 0.1, 0.3 and 0.6, respectively. The errors in brackets are derived from the 95% confidence intervals for ln(A) and E, estimated from linear fits to Arrhenius plots.

	Parameter	X=0.1	X=0.3	X=0.6
H_2	A/m s^{-1}	0.37 (−0.24,+0.65)	2.37 (− 1.66,+5.60)	1.59 (−1.43, +14.3)
	E/kJ mol^{-1}	62 (± 9)	78 (± 11)	79 (± 22)
CO	A/m s^{-1}	0.70 (−0.55, +2.57)	0.26 (− 0.18, +0.61)	0.13 (− 0.11, +0.59)
	E/kJ mol^{-1}	83 (± 14)	71 (± 11)	66 (± 15)

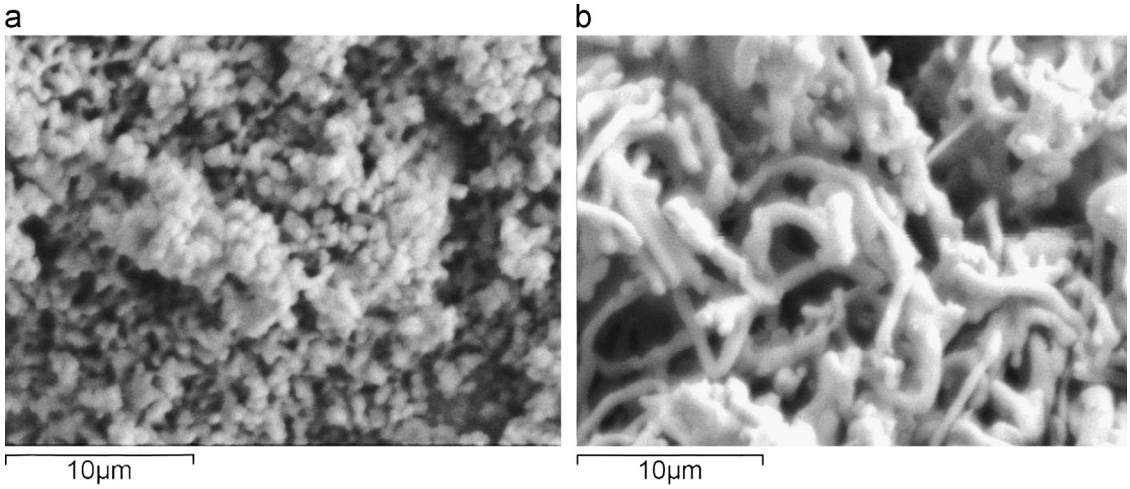

Fig. 13. Scanning electron microscope image of the surface of (a) an as-prepared wüstite particle (sieved to 300 to 425 μm), (b) a particle of wüstite after complete reduction in 4.95 vol% H_2 at 1123 K to metallic Fe.

5.2. Reaction mechanism during the reduction of wüstite by H_2

The results above suggest that the reduction of wüstite in H_2 undergoes three phases, with transitions around $X \approx 0.05$ and $X \approx 0.2$. In this section, the underlying mechanisms for these three stages are explored.

5.2.1. Reaction mechanism for the final stage with $0.2 < X < 1$

Here, more than 20% of the wüstite has been reduced to metallic iron. In that situation, the factors to be considered when formulating $f(X)$, which appears in Eq. (19), include: (i) the evolution of surface area, (ii) the evolution of the structure of pores (iii) the development of a product-layer, (iv) the diffusion of oxygen atoms through the product-layer and (v) exactly where the chemical reaction occurs. To investigate qualitatively the effects of (i) and (ii), the surface morphologies of the solid, before and after reduction in H_2, were examined using SEM; the images are shown in Fig. 13, which shows that the raw wüstite particles are fairly porous and are composed of small agglomerated solid grains with diameter ≈ 0.5 μm, similar to the diameter of the original, haematite powder. After reduction to Fe, the grains have formed long strings. Also, the overall porosity of the solid has increased, in accordance with the molar volume of Fe being 0.563 times that of wüstite. Based on Fig. 13, the random pore model, developed by Bhatia and Perlmutter (1981), taking into account chemical reaction between a gas and a solid, after diffusion through a layer of product, was investigated to see if it described the variation of rate with solid's conversion, X.

In the random pore model, the network of pores within a particle of wüstite is approximated by an assembly of randomly overlapping cylindrical pores, illustrated by Fig. 14 (b). The positions and orientations of the pores are random. This means that the volumes of the cylindrical pores can overlap in space, and are not necessarily parallel like those shown in Fig. 14 (b). In addition, it is assumed that, during reaction, the size of the porous particle (like the one in Fig. 14(a)), together with the total number of cylindrical pores and their length, are all constant. Thus, a chemically- reduced particle is much more porous than a fresh one, owing to the large changes in molar volume. Also the solid product remains continuously connected, eventually leading to a morphology resembling that seen in Fig. 13 (b).

The model describing the reaction zone is depicted in Fig. 14 (c) and assumes the following. When $X > 0.2$, a non-porous layer of Fe has formed on the walls of a pore. Then oxygen atoms diffuse from Fe_xO through Fe to the gas-solid interface to react with H_2, forming H_2O. By losing oxygen, Fe_xO thickens the layer of Fe, but the pore expands radially. This results in a constantly increasing resistance to the diffusion of O atoms through Fe and a maximum in the surface area at intermediate X (Bhatia and Perlmutter, 1980). Assuming no intra-particle concentration gradient in the gas phase, the rate of conversion of wüstite to iron can be expressed as a function of conversion, X (Bhatia and Perlmutter, 1981), as:

$$\frac{dX}{dt} = \left.\frac{dX}{dt}\right|_{\text{initial}} \times \frac{(1-X)\sqrt{1-\psi\ln(1-X)}}{1+\frac{\beta\alpha}{\psi}[\sqrt{1-\psi\ln(1-X)}-1]}, \tag{26}$$

$$\left.\frac{dX}{dt}\right|_{\text{initial}} = \frac{k_S S_0}{1-\varepsilon_0}\left([H_2]-\frac{[H_2O]}{K_{p4}}\right), \tag{27}$$

$$\beta = \frac{2k_S(1-\varepsilon_0)}{V_{FeO}S_0D_{s,O}}, \tag{28}$$

$$\psi = \frac{4\pi L_0(1-\varepsilon_0)}{S_0^2}, \tag{29}$$

Here k_S is an intrinsic rate constant describing dX/dt, expressed per unit area at the reaction interface on the wall of a pore. The rate constant k_S is different from k_A, which refers to the rate of reaction in mol s^{-1}. The definitions of various rate constants mentioned in the text are presented, together with their conversion factors in

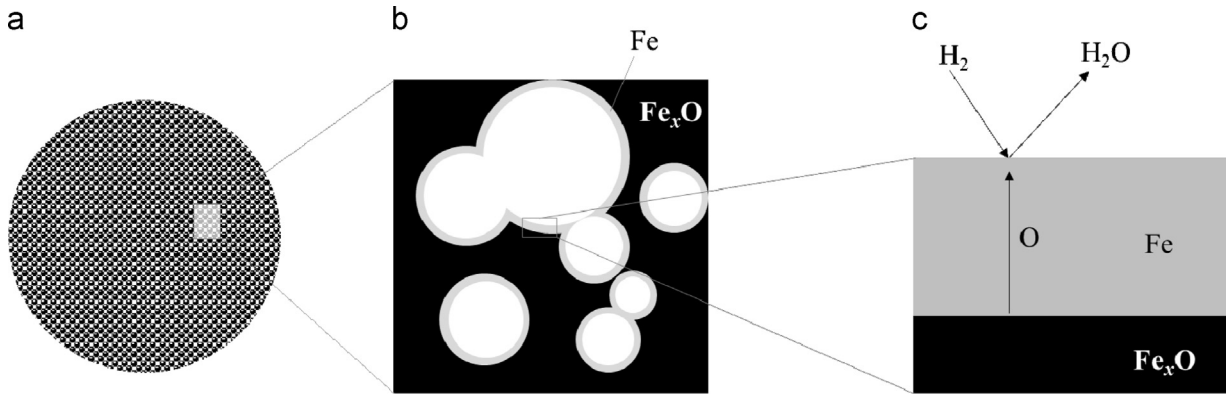

Fig. 14. Schematic diagrams of the random pore model, showing three levels of magnification: (a) a porous particle, (b) the cross-section of several parallel pores, which can overlap, and (c) a cross-section of the reaction front. The unreacted Fe_xO, the product Fe and the pore are in black, grey and white, respectively.

Table 2
Conversion between various rate constants.

Description	Symbol	Dimension	Conversion to k_i
Intrinsic rate constant per unit volume	k_i	s^{-1}	$\times 1$
Apparent rate constant	k_a	$m^3\,g^{-1}\,s^{-1}$	$\times f(X)/\rho_{FeO}$
Intrinsic rate constant per unit area for rate of reaction	k_A	$m\,s^{-1}$	$\times f(X)/S_0$
Intrinsic rate constant per unit area for rate of conversion	k_S	$m^4\,mol^{-1}\,s^{-1}$	$\times 14.69\rho_{FeO}S_0/(1-\varepsilon_0)$

Table 2. Also, V_{FeO} is the molar volume of wüstite, S_0 is the initial surface area per unit volume of the particle, $D_{s,O}$ is the diffusivity of oxygen ions through the product Fe, L_0 is the initial total length of overlapped pores per unit volume of particle and ε_0 is the initial porosity of the material. The dimensionless group β is a modified Biot number for the ratio of the rates of chemical reaction and of diffusion through the solid product; finally ψ is a structural parameter, characterising the degree of overlap of the pores in the initial porous structure prior to reaction.

One of the input parameters to the model, *viz.* the initial porosity of the particle, $\varepsilon_0=0.6$, was determined from an experimental estimate of the bulk density of a particle of wüstite. Three parameters which could not be measured directly, were determined by finding the best fit of the predictions from modelling to the experimental measurements at 1173 K for $X>0.2$. These three parameters are: the structural parameter, ψ, the rate constant, k_S and the coefficient of diffusion of oxygen ions in Fe, $D_{S,O}$. By using the Matlab curve fitting toolbox with the "Trust-Region" algorithm (MATLAB, 2008), the values of ψ, k_S and $D_{S,O}$ were found to be 10 ± 1, $(1.3\pm0.1)\times10^{-8}\,m^4\,mol^{-1}\,s^{-1}$ and $(1.0\pm0.5)\times10^{-11}\,m^2\,s^{-1}$, respectively; the result of the fit of some modelled rates to measured ones is shown in Fig. 15.

Now, the plausibility of the values of $D_{S,O}$ and ψ determined from the model will be investigated. Takada and Adachi (1986) calculated the diffusivity of oxygen ions through pure α-iron to be:

$$D_{s,O}=\left(2.91\,^{+3.40}_{-1.57}\right)\times10^{-7}\times\exp\left(\frac{-90\pm7\ \text{kJ mol}^{-1}}{RT}\right)\ \text{m}^2\,\text{s}^{-1}. \quad (30)$$

At 1173 K, Equation (30) gives $D_{s,O}=3.0\times10^{-11}\,m^2\,s^{-1}$, a value three times that found above from fitting the pore model. It is likely that the Fe produced in the current study is fairly different to the samples prepared by Takada and Adachi (1986) in terms of composition of impurities and density of grain-boundaries, both of which could alter $D_{s,O}$ substantially, but probably within the order of magnitude of 10^{-11} to $10^{-10}\,m^2\,s^{-1}$. Therefore, the estimated value of $D_{s,O}$ appears plausible. In addition, Takada and Adachi (1986) found that the effect of an impurity does not change the activation energy for $D_{s,O}$ significantly; therefore, the activation energy of 90 ± 7 kJ mol^{-1}, together with the corresponding pre-exponential factor of $1\times10^{-7}\,m^2\,s^{-1}$, were used to estimate $D_{s,O}$, as an input to the pore model, to simulate the reduction at different temperatures.

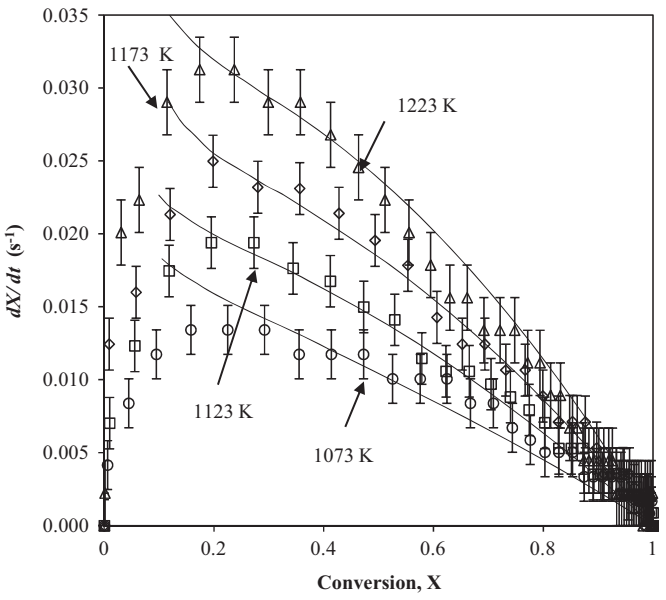

Fig. 15. Comparison of dX/dt from experimental measurements, to the results of modelling using the random pore model for the reduction of wüstite in 4.95 vol% hydrogen in N_2 at different temperatures. The lines are the results of modelling, and the points represent experimental measurements without smoothing. The error bars correspond to errors in individual measurements due to limits of detection of the gas analysers. For clarity, not all unsmoothed results are shown: one in every five, four, three and two measurements are plotted for 1073, 1123, 1173 and 1223 K, respectively.

An experimental determination of ψ requires quantitative information on the distribution of pore size within wüstite; alas,

such information was not available. However, the results of mercury intrusion porosimetry of Fe_2O_3 were used as a reference to check the estimate of $\psi \sim 10$. Because the molar volume of haematite is 1.2 times that of wüstite, the pore size distribution of haematite should be fairly close to that of wüstite, assuming no sintering. Based on the porosimetry results shown in Fig. 16, L_0 for Fe_2O_3 was estimated using:

$$L_0 = \frac{1}{\pi}\int_0^{\infty} \frac{v_{\text{pore}}}{r_{\text{pore}}^2} dr_{\text{pore}}, \tag{31}$$

given by Bhatia and Perlmutter (1980). Here v_{pore} is a pore volume distribution function in m^{-1} and r_{pore} is a pore's diameter in m. This gives $L_0 = 7.5 \times 10^{12}\ m^{-2}$. Also, the BET surface area was measured to be $1.0 \pm 0.5\ m^2\ g^{-1}$, *i.e.* $S_0 \approx (2.5 \pm 1.2) \times 10^6\ m^{-1}$. Using Eq. (29), the value of ψ was found to be 6 ± 3. Therefore, the estimate of $\psi = 10$ for wüstite particles, deduced above from the pore model is reasonable.

At temperatures other than 1173 K, the values of k_S were determined by fitting the model to experimental results, using the values of $D_{s,O}$ calculated from: $D_{s,O} = 1.0 \times 10^{-7} \exp[(-90\ \text{kJ mol}^{-1})/RT]\ m^2\ s^{-1}$ and $\psi = 10$ as the inputs to the model. All the results of modelling are compared to experimental measurements in Fig. 15. Evidently, there is good agreement between the experimental and theoretical plots in Fig. 15, which includes experimental errors. The Biot moduli, β, were calculated using the k_S and $D_{s,O}$ determined at various temperatures; the results are tabulated in Table 3. The good agreement between modelling and experiment in Fig. 15 means that, at least for these fairly large X, the random pore model is a serious possibility.

Using the values of k_S summarised in Table 3, the Arrhenius expression:

$$k_S = 7 \times 10^{-6} \exp\left(\frac{-62\ \text{kJ mol}^{-1}}{RT}\right) m^4\ \text{mol}^{-1}\ s^{-1}, \tag{32}$$

can be derived. Here, the 95% confidence bounds of $7\ (+44, -6) \times 10^{-6}\ m^4\ \text{mol}^{-1}\ s^{-1}$ and $62 \pm 19\ \text{kJ mol}^{-1}$ for A and E, respectively,

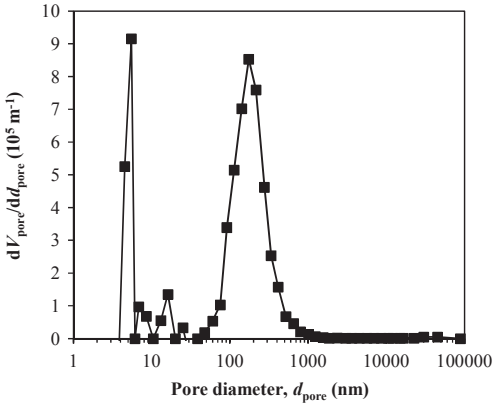

Fig. 16. Distribution of pore volume versus pore diameter of granulated haematite particles (d_p = 300–425 μm) measured by mercury intrusion porosimetry.

Table 3
Estimates of β at different temperatures for the reduction of wüstite in H_2 for $X > 0.2$

T K	$D_{s,O}$ $10^{-11}\ m^2\ s^{-1}$	k_S $m^4\ \text{mol}^{-1}\ s^{-1}$	β (dimensionless)
1073	0.4	7×10^{-9}	18
1123	0.7	9×10^{-9}	15
1173	1.0	1.3×10^{-8}	14
1223	1.5	1.6×10^{-8}	12

are extracted from the confidence bounds of the fitted parameters the Arrhenius plot. The uncertainty bands for A and E are larger than for parameters given previously, which is reflective of the relatively large scatter of points about the best fit line in the Arrhenius plot. Therefore, the activation energy of $78 \pm 11\ \text{kJ mol}^{-1}$, measured for the intrinsic rate constant, k_A, in Section 4.2, is the result of combining the rates of: (i) diffusion of oxygen ions through Fe (with a activation energy of $90 \pm 7\ \text{kJ mol}^{-1}$) and (ii) chemical reaction (with an activation energy of $62 \pm 19\ \text{kJ mol}^{-1}$).

Table 3 also shows that β decreases with increasing temperature. This is because k_S has a lower activation energy than $D_{s,O}$. Nevertheless, the fact that $\beta > 10$ over the temperatures studied indicates that diffusion through the product-layer, rather than chemical reaction, is the dominant factor in determining how the rate of reaction varies with X.

As mentioned earlier, the random pore model considers the evolution of the microstructure of a porous particle and models the pores as cylindrical volume elements, whilst the solids occupy the space not occupied by the pores. Alternatively, another type of geometric simplification, which considers the solid phase as an assembly of agglomerated spherical grains, was proposed by Sotirchos and Yu (1988), for modelling gas–solid reactions. In a grain-based model, the structure of the porous solid can be characterised by a discretised distribution function for grain-sizes, as used by Liu et al. (2012b). However, this grain-approach is not applicable to the reduction of wüstite, because it assumes that the spherical grains of the reactant wüstite remain spherical throughout the reaction, which is not particularly the case here, as depicted in Fig. 13. In addition, the so-called "overlapping grain model" assumes that the grains are randomly positioned in space; this is also not a good assumption in the current case, where both the pores and the solid phase are continuously connected.

5.2.2. *Reaction mechanism for the initial stage with $X < 0.05$*

It was noted above, that there is an initial phase, where the rate of reaction reaches an approximately constant level at $X \sim 0.05$. This initial stage is most likely to be associated with the depletion of lattice oxygen in wüstite prior to the formation of Fe: a process inevitable during the reduction of wüstite (John et al., 1984). This can be explained as follows. Wüstite crystals contain p-type metal defects (cationic deficits). In fact, the value of δ in the chemical formula for wüstite, $Fe_{1-\delta}O$, is a function of temperature and the redox potential at the gas-solid interface. According to the correlation by Giddings and Gordon (1973), $\delta = 0.067$ for the wüstite particles used in this study, whereas the value of δ is between 0.053 and 0.049 at the wüstite-Fe phase boundary between 923 K and 1223 K. As a result, there occurs an initial reaction, in which the lattice oxygen in wüstite is quickly depleted and the value of δ is slightly reduced, before there is a phase-change from wüstite to Fe. This initial reaction (typified at 923 K by $Fe_{0.933}O + 0.0148H_2 \rightarrow 0.985Fe_{0.947}O + 0.0148H_2O$) is responsible for $\sim 2\%$ of the total conversion. In addition, it is possible that this reaction overlaps with the subsequent nucleation of Fe, resulting in the observed, approximately constant-rate region at around $X \sim 0.05$. However, it was difficult to study the kinetics of this first phase, especially at high temperature when the reaction was rapid, owing to the limited sampling frequency of the gas analysers. The same holds for the reduction of wüstite in CO when $0 < X < 0.05$, as depicted in Fig. 11. Even so, the measurements in Fig. 8 did enable very rough estimates to be made of $A \approx 9\ m\ s^{-1}$ and $E = 96 \pm 7\ \text{kJ mol}^{-1}$ for this initial reaction with H_2 and $A \approx 13\ m\ s^{-1}$ and $E = 111 \pm 7\ \text{kJ mol}^{-1}$ for that with CO. These differing estimates of E indicate that the initial rates are not controlled by diffusion of Fe^{2+} ions in $Fe_{1-\delta}O$, whose activation energy is $29 \pm 1\ \text{kJ mol}^{-1}$ (Chen and Peterson, 1975), but instead, by a chemical reaction.

5.2.3. Reaction mechanism for the second stage with $0.05 < X < 0.2$

Fig. 17 shows a proposed mechanism for the second stage (assumed to be $0.05 < X < 0.2$) when product-islands of Fe nucleate and grow over the surface of wüstite. Because the adsorption energy of H_2 on metallic Fe ($\Delta H_{ads} = 150$ kJ mol^{-1}) is much greater than on magnetite (Fe_3O_4, $\Delta H_{ads} = 80$ kJ mol^{-1}) (Geus, 1986; Van der Laan, Beenackers, 1999), it is anticipated that H_2 is also adsorbed more strongly on Fe than on FeO. It has also been observed that iron surfaces, which have been covered with oxygen, have lower binding energies for CO and H_2 than surfaces on which nothing has been adsorbed. In addition, the presence of oxygen on the surface may inhibit the dissociation of H_2 (Benziger and Madix, 1980) there. One result is that the rate of adsorption of CO or H_2 on Fe is much faster than on FeO. This means that, when there is Fe present on the surface, the reduction of wüstite by H_2 mainly undergoes the following processes: (i) dissociative adsorption of hydrogen on islands of Fe, (ii) migration of adsorbed H atoms from Fe to a reaction site, (iii) chemical reaction between H (ads) and O(ads) atoms and (iv) desorption of H_2O from the surface. Process (iii) involves reaction between H(ads) and O atoms, which have diffused through the product-layer in process (v). Such reaction occurs either on wüstite adjacent to Fe or (via the mechanism depicted by Fig. 14(c)) at active sites on the surface of iron. However the reaction via this latter route is much slower, because the rate of diffusion of hydrogen atoms on Fe (process ii) is four orders of magnitude faster than the rate of diffusion of O atoms through Fe (process v), as shown by the analysis in the Appendix. On a surface free of Fe, direct reaction between wüstite and H_2 is also possible, *via* steps (i), (iii) and (iv), but at a much slower rate, for the reasons explained above. Similar considerations have been given by Li et al. (2012), who proposed a mechanism for the carbonation of CaO, taking into account adsorption and diffusion on the surface. However, in Li et al. (2012) mechanism, the gaseous reactants adsorb on the unreacted solid and molecules or islands of product are the diffusing species on the surface.

Therefore, it is hypothesised here, that for $0.05 < X < 0.2$, the overall reaction is controlled by the dissociative adsorption of H_2, facilitated by the growing surface area of the product Fe. At $X \approx 0.2$, the rate-determining step progressively becomes that of the growth of a layer of Fe and the rate can be expressed using the pore-model described in Section 5.2.2. As explained above, because the rate of diffusion of H atoms on Fe is much faster than the rate of diffusion of O^{2-} through Fe, the product-islands are more likely to grow in directions parallel to the surface, resulting in a layer of Fe of approximately uniform thickness covering the surface of wüstite.

Thus, the initial rate-determining step, *i.e.* the rate of adsorption, can be written, in mol g^{-1} s^{-1}:

$$r_1 = \frac{k_{ads1}}{\rho_{FeO}}\left([H_2]_g - \frac{[H]^2_{ads}}{K_{ads,H_2}}\right)\frac{S_0}{(1-\varepsilon_0)}\gamma. \tag{33}$$

Here k_{ads1} (in m s^{-1}) is a rate constant for adsorption, $[H_2]_g$ is the concentration of hydrogen in the gas phase, $[H]_{ads}$ is the concentration of adsorbed hydrogen atoms, $K_{ads,H}$ is the equilibrium constant for the adsorption of hydrogen, $S_0/(1-\varepsilon_0)$ is the specific surface area per unit volume of solid in m^{-1}, and γ is the fractional coverage of the surface by metallic Fe.

By assuming $[H]_{ads}$ is at a steady state, the concentration driving forces for processes (iii) and (iv) are $([H]^2_{ads}[O]_{ads} - [H_2O]_{ads}/K_{e1})$ and $([H_2O]_{ads} - K_{ads,H2O}[H_2O]_g)$, respectively. The symbols $[O]_{ads}$, $[H_2O]_{ads}$, K_{e1}, $K_{ads,H2O}$, and $[H_2O]_g$ represent, respectively, the concentration of oxygen atoms on the surface, the concentration of adsorbed H_2O, the equilibrium constant for the surface reaction, equilibrium concentration for adsorption of H_2O and finally, the concentration of H_2O in the gas phase. Assuming the overall process is controlled by surface adsorption, $([H]^2_{ads}[O]_{ads} - [H_2O]_{ads}/K_{e1}) \approx 0$, $([H_2O]_{ads} - K_{ads,H2O}[H_2O]_g) \approx 0$ and $[O]_{ads}$ is a constant, the rate expression for the dissociative adsorption of H_2 on Fe is:

$$r_1 = \frac{k_{ads1}S_0\gamma}{(1-\varepsilon_0)\rho_{FeO}}\left([H_2]_g - \frac{K_{ads,H_2O}}{K_{e1}[O]_{ads}K_{ads,H_2}}[H_2O]_g\right). \tag{34}$$

The term $K_{ads,H2O}/K_{e1}[O]_{ads}K_{ads,H2}$ is in fact K_{p4} in this model. Because a similar expression can be written for the rate of adsorption on a surface of wüstite, the overall rate, when controlled by dissociative adsorption, is:

$$r' = \frac{([H_2]_g - [H_2O]_g/K_{p4})S_0}{(1-\varepsilon_0)\rho_{FeO}}[k_{ads1}\gamma + k_{ads2}(1-\gamma)], \tag{35}$$

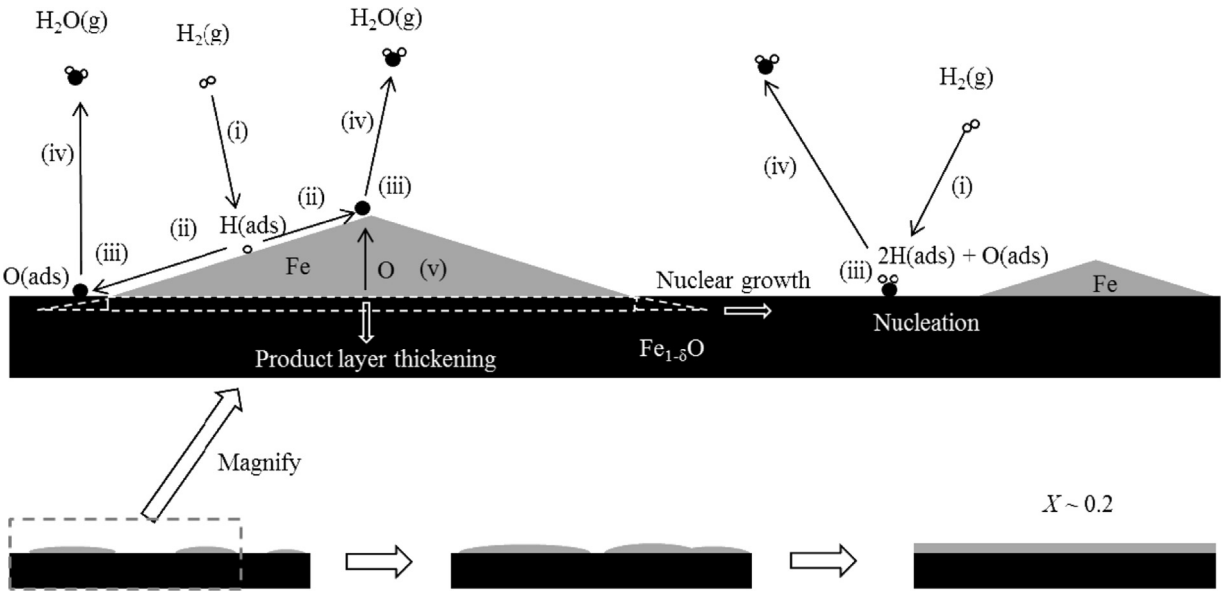

Fig. 17. Sketch of the reduction of wüstite in hydrogen at low conversions. The arrows are numbered to represent the following: (i) dissociative adsorption of H_2 onto the surface, (ii) diffusion of H atoms on surface of Fe, (iii) chemical reaction between adsorbed H and O atoms, (iv) desorption of H_2O from surface, and (v) diffusion of O atoms through Fe. In case where hydrogen adsorbs on surface of wüstite, steps (i), (iii) and (iv) are applicable.

where k_{ads2} is the rate constant for the adsorption of H_2 on wüstite. Solving Eq. (35) requires a relationship between γ (fractional coverage of the surface of Fe) and X. Under the simplifying assumption that the product-layer is of uniform thickness, γ varies proportionally with conversion, taking into account the first 2% of conversion, which does not yield Fe. Therefore, the second term in Eq. (35), *i.e.* $k_A(1-\varepsilon_0)$, should vary linearly with X. To derive an approximate expression for k_A as a function of X, a plot of k_A versus X (*e.g.* Fig. 7) is fitted by a straight line, for $0.05 < X < 0.2$, at 1173 K. From the linear fit (not shown here), k_A was found to be directly proportional to $(X+0.13)$. Also the apparent activation energy of this process is 62 ± 9 kJ mol^{-1}, as measured in Section 4.2. By introducing a combined rate constant, $k_{S,I}$, with the same dimension as k_S in the pore model in Section 5.2.1, γ can be approximately related to X by:

$$k_{S,I}(X+0.13) = \frac{k_{ads2} + (k_{ads1} - k_{ads2})\gamma}{\rho_{FeO} \times 0.01469 \text{ mol g}^{-1}}, \quad (36)$$

where the coefficient $1/(0.01469 \text{ mol g}^{-1})$ converts the specific rate of reaction, r' to conversion, X. Assuming $X=0.2$ when $\gamma=1$, then Eq. (36) implies that $k_{ads2}/k_{ads1}=0.39$, which is in agreement with the initial proposition that the rate of adsorption of H_2 on metallic Fe is much faster than that on wüstite. By writing $k_{S,I}$ in an Arrhenius expression, the rate of conversion in the second stage can be expressed at every temperature, T, as:

$$\frac{dX}{dt} = 2 \times 10^{-5} \exp\left(\frac{62 \pm 9 \text{ kJ mol}^{-1}}{RT}\right) \times \frac{([H_2]_g - [H_2O]_g/K_{p4})S_0}{1-\varepsilon_0}(X+0.13). \quad (37)$$

The results of modelling the rates in the second stage at different temperatures using the parameters extracted at 1173 K are compared to experimental results in Fig. 18. The fits up to $X \sim 0.15$ are good. The fact that the simplified model is capable of predicting profiles of $k_i f(X)$ calculated from experimental results at various temperatures suggests that the initial rate is indeed of first order with respect to $([H_2]-[H_2O]/K_{p4})$. However, the activation energy assumed for adsorption (62 ± 9 kJ mol^{-1}) is higher than those reported in the literature, *e.g.* 43 kJ mol^{-1} (Berger et al., 1992) and 15 kJ mol^{-1} (Sorescu, 2005), for the dissociative adsorption of H_2 on Fe (1 0 0). Nevertheless, this difference in activation energy is not unexpected, because most measurements or theoretical calculations of the activation energy for the adsorption of hydrogen on Fe were performed over the temperature range 200–500 K, and show large variations amongst authors.

5.3. Reaction mechanism for reduction with CO

Similar to the reduction in hydrogen, different activation energies were found for $X=0.1$ and $X=0.3$ or 0.6, when particles of wüstite were reduced in CO. As discussed in section 5.2.2 and Fig. 8, the initial 5% of conversion involves the initial reaction, in which the oxygen-content in the wüstite is depleted. This initial reaction is not investigated further here. Attention is accordingly directed to the other two stages from $X \sim 0.05$ to $X \sim 0.2$ and then up to $X=1$. In this case, the transition between these two regimes of reaction might not be at the maximum in rate, when $X=0.3$, because of the similarities in the activation energies of k_A measured at $X=0.3$ and 0.6, in section 4.3. From the SEM images of particles of wüstite before and after complete reduction in CO, shown in Fig. 19, it can be seen that there is considerable similarity in morphology between the sample reduced in H_2 (shown in Fig. 13) and that in CO (Fig. 19). Therefore the random pore model is also employed here to describe the rate for $X > 0.2$, using Eqs. (26–28). In this case, H_2 is replaced by CO and H_2O by CO_2; the value of $K_{p7}=p_{CO_2}/p_{CO}$ was calculated from the thermodynamic properties given by Barin (1973). An analysis similar to section 5.2.2 was undertaken to estimate the input parameters to the model. The structural parameters, ψ and ε_0, which are independent of the gaseous species, were kept the same as those estimated in section 5.2.2. The diffusion of oxygen ions through Fe was again considered the only type of mass transfer, which might substantially influence the overall rate of conversion. The value of $D_{s,O}$ was kept the same as that determined in section 5.2.2. Also, the rate constant describing the rate of conversion of wüstite per unit surface area, $k_{S,}$ was determined by fitting equations equivalent to (26)–(28) for CO, to rates, measured at different temperatures, as shown in Fig. 20.

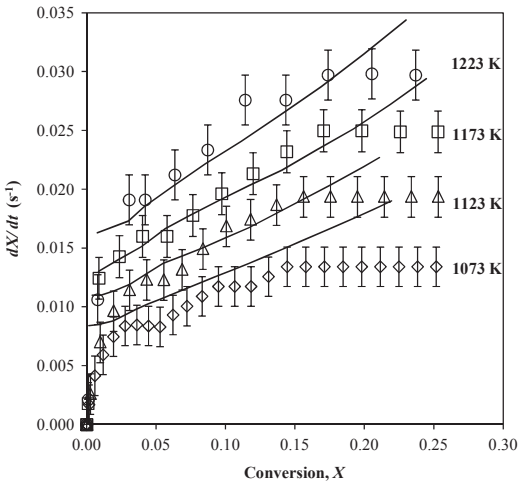

Fig. 18. Comparison of dX/dt against X measured from experiments, with those calculated using a linear correlation to describe the rate in the second stage, for $0 < X < 0.20$, for the reduction of wüstite in 4.95 vol% hydrogen in nitrogen at different temperatures. The lines represent the results of modelling, and the points represent experimental measurements without smoothing. The error bars correspond to errors in individual measurements. The time-interval between consecutive plotted points is 1 s for all temperatures.

The values of k_S determined from the pore model are tabulated in Table 4. Using these values, the temperature dependence of k_S can be expressed as the Arrhenius equation:

$$k_S = 1.1 \times 10^{-6} \times \exp\left(\frac{-64 \text{ kJ mol}^{-1}}{RT}\right) \text{m}^4 \text{ mol}^{-1} \text{ s}^{-1}. \quad (38)$$

Here, the 95% confidence bounds of 1.1 $(+1.6, -0.8) \times 10^{-6}$ m^4 mol^{-1} s^{-1} and 64 ± 8 kJ mol^{-1} for A and E, respectively, are extracted from the confidence bounds of the fitted parameters the Arrhenius plot. The smaller error bounds mean that there was less scatter on the Arrhenius plot and a better fit was achieved. Accordingly, the values of β (ratio of rates of chemical reaction and diffusion through the product, Fe) calculated at various temperatures are also shown in Table 4, from which it can be seen that the value of β for the reduction of wüstite in CO is approximately 1/8 of that for reduction in hydrogen. This is because the pre-exponential factor for k_S for reduction in hydrogen is ~ 8 times that for CO, whereas the activation energies estimated in both cases are almost identical. This difference in the value of β is responsible for the differences in the shapes of the rate profiles for the two reactions (*e.g.* Figs. 7 and 11).

From Fig. 20, it can be seen that, the pore model predicts a maximum rate when $X \sim 0.3$ at 1173 K and 1123 K, whereas at lower temperatures the rate reaches a plateau for X between 0.2 and 0.4; these predictions are in agreement with the experiments, taking into account the experimental errors owing to the limited resolution of the raw measurements. According to the pore model, the maximum rate measured at $X \sim 0.3$ was a result of a maximum in surface area during the evolution of the pore structure. This maximum is not seen with H_2 as reductant, owing to the effect of a high β, as discussed by Bhatia

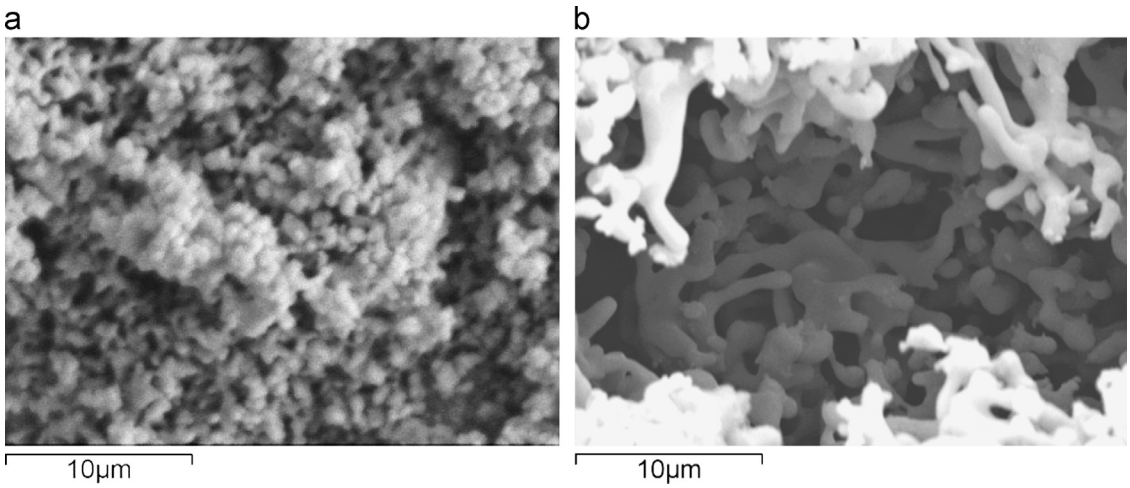

Fig. 19. Scanning electron microscope image of the surface of (a) an as-prepared wüstite particle, (b) a particle of iron after reduction of wüstite to $X=1$ in 9.7 vol% CO at 1073 K in a fluidised bed.

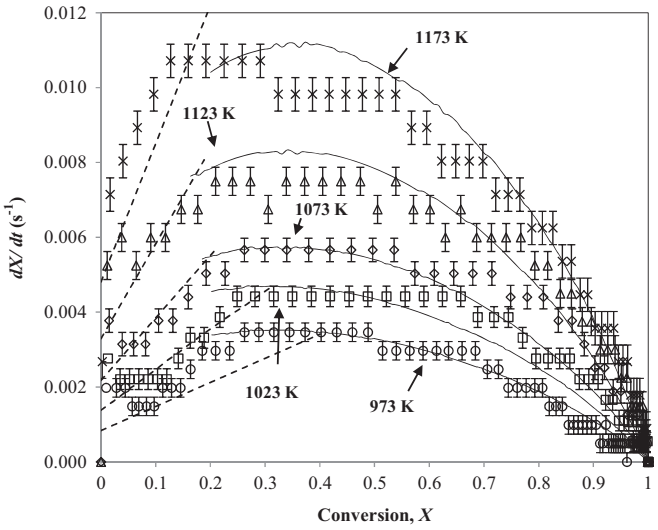

Fig. 20. The rates of reaction plotted against conversion when a small batch of wüstite particles, $d_p=300$–425 μm was reduced in 9.7 vol% CO in N_2 at different temperatures between 973 K and 1173 K. The dashed lines represent the results of modelling the initial rate of reaction for $0.05<X<0.2$, the solid lines represent the results of a random pore model with $\psi=10$, and the points represent measurements without smoothing. The error bars correspond to errors in individual measurements. For clarity, not all unsmoothed results are shown: one in every seven, six, five, four and three measurements are plotted for 973, 1023, 1073, 1123 and 1173 K, respectively.

and Perlmutter (1981). Therefore it is probable that the transition between the two stages of reaction with CO occurs not at $X\sim0.3$ but at $X\sim0.2$, just as with H_2.

Similar to hydrogen, CO adsorbs on Fe more strongly ($\Delta H_{ads}=145$ kJ mol^{-1}) than on the oxides of iron, *e.g.* $\Delta H_{ads}=113$ kJ mol^{-1} for adsorption of CO on Fe_3O_4 (Udovic and Dumesic, 1984; van der Laan and Beenackers, 1999). Accordingly, the same surface-adsorption hypothesis was used to describe the kinetics at $0.05<X<0.2$, as in section 5.2.3. Again, the correlation between dX/dt and X was approximated by a straight line of best fit to the experimental results at 1123 K for $0.05<X<0.2$, with a rate constant $k_{S,I}$ in m^4 mol^{-1} s^{-1} as shown in Fig. 20. This linear correlation, where the rate was again proportional to $(X+0.13)$, was also applied to different temperatures, using a rate expression equivalent to eq. (37) with $k_{S,I}=(3.0\pm0.5)\times10^{-5}\ \exp[(-83\pm14\ \text{kJ mol}^{-1})/RT]$ m^4 mol^{-1} s^{-1}, where 83 kJ mol^{-1} is the activation energy determined from the rate constants measured at iso-conversion points of $X=0.1$, as described in section 4.3. This activation energy is lower than the value of 105 kJ mol^{-1} reported by Benziger and Madix (1980), who measured the adsorption of CO on Fe(100) surfaces. Given that, in practice, CO would adsorb on various crystallographic planes of iron, this difference in activation energy is acceptable. It can be seen from Fig. 20 that the linear correlation and the random pore model predict reasonably well the rates of reaction at various operating conditions for the reduction of wüstite to Fe in CO for $0.05<X<0.2$ and $0.2<X<1$, respectively.

Table 4
Estimates of β at different temperatures for modelling the reduction of wüstite in CO for $X>0.2$ using a random pore model.

T K	$D_{s,O}$ 10^{-11} m^2 s^{-1}	k_S m^4 mol^{-1} s^{-1}	β (dimensionless)
973	0.16	4×10^{-10}	3
1023	0.27	6×10^{-10}	2
1073	0.44	8×10^{-10}	2
1123	0.69	1.1×10^{-9}	2
1173	1.0	1.6×10^{-9}	2

5.4. Simultaneous reduction of wüstite in CO and H_2

Finally, wüstite particles were reduced in three mixtures of CO and H_2, with N_2 as the balancing gas at 1123 K. The composition of the gas mixture was adjusted to vary the rate of reduction by the two gases, whilst keeping the overall flowrate roughly the same, nominally at 2.5 L min^{-1} (at 295 K, 1 atm). The concentration of CO was ~12, 6 and 3 times that of H_2 in the three mixtures, so that the corresponding rates of reactions with CO were expected to be approximately 4, 2 and 1 times that of H_2. These rates were estimated assuming H_2 and CO reacted independently, according to the kinetic parameters derived in Sections 4.2 and 4.3, when only H_2 or CO was present with N_2. The rates measured for reducing wüstite with H_2 and CO yielded the specific rates of consumption of H_2 and CO, denoted r'_{H_2} and r'_{CO}, according to the conventions used in Eq. (11) and its equivalent for CO. A reduced specific rate constant, k'_s, which is a function of X, was calculated using equations (39)–(41); x in Eq. (41) is the ratio of Fe:O at the wüstite-iron phase boundary at the corresponding temperature. The profiles of k'_s are plotted in Fig. 21 and are compared with the cases when only one gaseous reactant was present.

$$r'_{H_2}=\frac{k'_{s,H_2}}{\rho_{FeO}}\left([H_2]-\frac{[H_2O]}{K_{p4}}\right)\exp\left(-\frac{E_{A,H_2}}{RT}\right), \tag{39}$$

$$r'_{CO} = \frac{k'_{s,CO}}{\rho_{FeO}}\left([CO] - \frac{[CO_2]}{K_{p7}}\right)\exp\left(-\frac{E_{A,CO}}{RT}\right), \quad (40)$$

$$X = (56x+16)\int_0^t r'_{H_2} + r'_{CO}\,dt. \quad (41)$$

From Fig. 21 it can be seen that, when both CO and H_2 were present, the reduced specific rate constants, which varied with X in both cases, were the same as in the cases when only one species was present. This experimental observation suggests that there is no synergy between the two reactions. It is reminded that, the reaction model for $0.05 < X < 0.2$ assumes effectively low surface coverage by CO and H_2, so that the competition for adsorption sites between H_2 and CO is not expected here. Therefore the reaction models derived for H_2 and CO in sections 5.2 and 5.3 above are also applicable when particles of wüstite are reduced in one of their mixtures. In other words, when wüstite is reduced simultaneously by H_2 and CO, the total rate of reduction of wüstite equals to $(r'_{H2} + r'_{CO})$, as calculated using equations (39)–(41). This finding is particularly useful for designing reactors for the chemical looping production of hydrogen, when syngas consisting of CO and H_2 is used as the feed to the fuel reactor.

According to the reaction models developed in sections 5.2 and 5.3, at low conversions, both reactions are controlled by the surface adsorption of gaseous reactant until $X \sim 0.2$. When $X > 0.2$, the falling rates of reactions, can be predicted by a random pore model, with input parameters including: the rate constant k_S, the coefficient of diffusion of O^{2-} in Fe, $D_{s,O}$, the gaseous concentration driving force and the structural parameter ψ characterising the pore network. These parameters are unaffected by the presence of both H_2 and CO, since they consume the unreacted solid simultaneously. The product Fe, which forms a shell on the exterior of the wüstite, gives rise to a resistance from diffusion through this product. Using the pore model, which takes into account both the chemical reactions and diffusion through the product-layer, the difference between the rates of reduction of wüstite in H_2 and that in CO can be explained by a difference in the effective Biot moduli, β.

The pre-exponential factors and activation energies for various rate constants, k_S, derived above, are summarised in Table 5. After converting the units of the pre-exponential factor, A, to m s^{-1}, it is confirmed that values of A estimated from k_S are less than those predicted by collision theory.

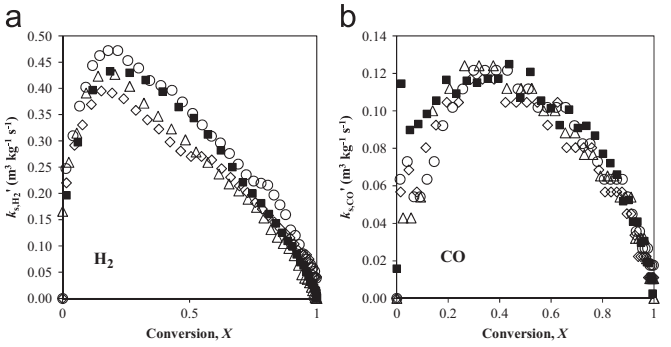

Fig. 21. Smoothed profiles of specific rate constants k'_s for the oxidation of (a) H_2 and (b) CO by wüstite, *versus* conversion of wüstite to Fe at 1123 K in gases containing various ratios of H_2 to CO. The symbols Δ, ◇ and ○ represent the results from different experiments in which the rate of reaction with CO is 1, 2 or 4 times that with of H_2. Changes in the rates of reaction were made by altering the concentrations knowing both reactions are of first order. The black squares represent the cases when wüstite is reduced solely by H_2 or CO. For clarity, one in every five measurements was plotted, where the time interval between two consecutive measurements was 1 s; and error bars are not shown.

6. Conclusions

In this investigation, wüstite particles were reduced by H_2 or CO in a fluidised bed to produce metallic iron. Rates were measured, when controlled by intrinsic kinetics under isothermal conditions. It was observed that the reduction of wüstite in hydrogen or CO undergoes three consecutive phases of reaction. These three stages correspond to: (i) partial depletion of oxygen in wüstite, when $0 < X < 0.05$, (ii) surface nucleation and the growth of product-islands of Fe when $0.05 < X < 0.2$ and (iii) thickening of the product-layer of Fe when $0.2 < X < 1$. In this final stage, the kinetics of reduction of wüstite in hydrogen or carbon monoxide can be described using a random pore model. However, the rate at $0.05 < X < 0.2$ can be approximated by a linear correlation. The rate expressions for reducing wüstite to Fe in hydrogen and CO are, respectively:

$$\left.\frac{dX}{dt}\right|_{H_2} = \frac{S_0\left([H_2] - \frac{[H_2O]}{K_{p4}}\right)}{1-\varepsilon_0}\begin{cases} k_{S,I,H_2}(X+0.13) & \text{for } X \le 0.2 \\ \dfrac{k_{S,II,H_2}\sqrt{1-\psi\,\ln(1-X)}}{1+\frac{\beta_{H_2}\alpha}{\psi}[\sqrt{1-\psi\,\ln(1-X)}-1]} & \text{for } X > 0.2 \end{cases} \quad (42)$$

$$\left.\frac{dX}{dt}\right|_{CO} = \frac{S_0([CO] - ([CO_2]/K_{p7}))}{1-\varepsilon_0}\begin{cases} k_{S,I,CO}(X+0.13) & \text{for } X \le 0.2 \\ \dfrac{k_{S,II,CO}\sqrt{1-\psi\,\ln(1-X)}}{1+\frac{\beta_{CO}\alpha}{\psi}[\sqrt{1-\psi\,\ln(1-X)}-1]} & \text{for } X > 0.2 \end{cases}, \quad (43)$$

where $\beta_i = 2k_{S,II,i}(1-\varepsilon_0)/(V_{FeO}S_0D_{s,O})$ is a Biot modulus comparing the rates of chemical reaction and diffusion through Fe, when species i is the gaseous reductant; $k_{S,I,i}$ and $k_{S,II,i}$ are rate constants for $0.05\ X < 0.2$ and $X > 0.2$, respectively; $D_{s,O}$ is the coefficient of diffusion of oxygen ions in Fe. The temperature dependences of $k_{S,i}$ and $D_{s,O}$ were derived and are given in Tables 3 and 4.

When wüstite is reduced simultaneously by a mixture of hydrogen and carbon monoxide, the total rate of reduction of wüstite is the superposition of two non-interacting rates. This modelling approach, especially the modelling of the initial rates, has not been applied before to the kinetics of reactions in chemical looping. The difference between the shape of the rate-curves for the reduction in H_2 and that in CO is a result of the difference in the effective Biot moduli, β. Although the rate of reduction of wüstite in H_2 is much faster than in CO, it is also affected more by the slow diffusion of oxygen ions in Fe.

Table 5
Summary of the pre-exponential factors and activation energies for the rate constants, k_S, for modelling the reduction of wüstite particles in H_2 and CO.

	$0.05 < X < 0.2$			$0.2 < X < 1$		
	Pre-exponential factors, A''		E	Pre-exponential factors, A''		E_A
	10^{-5} m^4 mol^{-1} s^{-1}	m s^{-1}	kJ mol^{-1}	10^{-6} m^4 mol^{-1} s^{-1}	m s^{-1}	kJ mol^{-1}
H_2	2.0	1.8	62 ± 9	7	0.63	62 ± 19
CO	3.0	2.7	83 ± 14	1.1	0.099	64 ± 8

Nomenclature

$[CO]$ concentration of CO mol m^{-3}
$[H]_{ads}$ concentration of adsorbed hydrogen atoms mol m^{-2}
$[H_2O]_g$ concentration of steam in the gas phase mol m^{-3}
A pre-exponential factor for the Arrhenius expression for k_A m s^{-1}
A' pre-exponential factor for the Arrhenius expression for k_i s^{-1}
A'' pre-exponential factor for the Arrhenius expression for k_S m^4 mol^{-1} s^{-1}
A_0 catchment area of the distributor m^2
$C_{inlet\ (outlet)}$ inlet (outlet) concentration mol m^{-3}
D atomic diffusivity coefficient in a solid lattice m^2 s^{-1}
D_0 pre-exponential factor for atomic diffusion m^2 s^{-1}
D_{bulk} atomic diffusivity through the solid lattice m^2 s^{-1}
D_M molecular diffusivity m^2 s^{-1}
d_p diameter of a particle m
d_{pore} diameter of a pore nm
$D_{surface}$ atomic diffusivity over the surface of a solid lattice m^2 s^{-1}
$D_{s,O}$ diffusivity of oxygen ions through product-layer m^2 s^{-1}
E activation energy kJ mol^{-1}
H depth of a bed m
H_{mf} depth of a bed at minimum fluidisation m
h inter-phase heat transfer coefficient W m^{-2} K^{-1}
h' vertical distance upwards from a distributor m
k' first order rate constant in the crossflow factor model s^{-1}
k_A first order intrinsic rate constant based on area m s^{-1}
k_a apparent rate constant based on volume s^{-1}
$K_{ads,i}$ equilibrium constant for the adsorption of species i various
k_{ads} rate constant of adsorption per based on area m s^{-1}
K_{e1} equilibrium constant for reaction between H(ads) and O (ads) m^4 mol^{-2}
k_g external mass transfer coefficient m s^{-1}
k_i first order intrinsic rate constant based on volume s^{-1}
K_{pi} equilibrium constant of reaction i at temperature in Kelvin (dimensionless)
k_S intrinsic rate constant based on rate of conversion per unit area m^4 mol^{-1} s^{-1}
k_s' reduced specific rate of reaction s^{-1}
L_0 length of the pore system per unit volume m^{-2}
M_i molecular weight of species i g mol^{-1}
m_i mass of species i
$\dot{N}_i$ molar flowrate of species i mol s^{-1}
N_i number of moles of species i mol
$\dot{N}_{tot}$ total molar flowrate mol s^{-1}
Nu Nusselt number (dimensionless)
p_i partial pressure of species i bar
Q volumetric crossflow m^3
R universal gas constant, 8.314×10^{-3} kJ mol^{-1} K^{-1}
r' specific rate of reaction mol g^{-1} s^{-1}
r_1 rate of adsorption mol g^{-1} s^{-1}
R_0 external radius of a particle m
Re Reynolds number (dimensionless)
r_{pore} radius of a pore m
S_0 initial specific surface area of inside a particle m^{-1}
Sc Schmidt number (dimensionless)
Sh Sherwood number (dimensionless)
T temperature K
t time s
T_∞ temperature of the bulk particular phase K
t_d dead time of a PFR s
U superficial velocity m s^{-1}
U_b rise velocity of a bubble m
U_{mf} minimum fluidisation velocity m s^{-1}
V_b volume of a bubble m^3
V_{FeO} molar volume of wüstite m^3 mol^{-1}
V_{pore} specific pore volume (dimensionless)
w_i weight factor for the ith element in weighted linear regression (dimensionless)
X fractional solid conversion dimensionless
X solid conversion by species i (dimensionless)
X_{fl} crossflow factor (dimensionless)
$X_{Wüs}$ conversion of Fe_2O_3 to wüstite (dimensionless)
x ratio of Fe:O in wüstite (dimensionless)
y_{actual} deconvoluted mole fraction (dimensionless)
y_i mole fraction of gas species i (dimensionless)
$\dot{y}_{measured}$ derivative of $y_{measured}$ with respect to time (dimensionless)
$y_{measured}$ mole fraction measured by gas analyser (dimensionless)

Greek Symbols

α ratio of the molar volume of solid product to reactant (dimensionless)
β Biot number in a random pore model (dimensionless)
γ fractional surface coverage by the product layer (dimensionless)
ΔH_{ads} heat of adsorption J mol^{-1}
ΔH_T^o standard enthalpy of reaction at temperature T in Kelvin J mol^{-1}
Δy_i a step change of mole fraction of species i in the inlet (dimensionless)
δ fractional lattice deficiency (dimensionless)
ε_0 initial porosity of the particle (dimensionless)
ε_{mf} voidage of the fluidised bed at minimum fluidisation (dimensionless)
η effectiveness factor
λ_e effective thermal conductivity of the porous particle W m^{-1} K^{-1}
υ kinematic viscosity m^2 s^{-1}
ρ_{FeO} mass density of wüstite g m^{-3}
ρ_{solid} mass density of the solid reactant g m^{-3}
τ_M characteristic mixing time in a CSTR s
υ_{pore} specific pore volume distribution as a function of pore diameter m^{-1}
ψ structural parameter in a random pore model (dimensionless)
ω $1 - U_{mf}/U$ (dimensionless)

Acknowledgement

The author would like to thank Mr. Simon Griggs with SEM, and Mr Zlatko Saracevic with BET and mercury intrusion porosimetry measurements. Financial support from the Engineering and Physical Sciences Research Council (Grant number: EP/G063265/1) is also acknowledged.

Appendix. Order of magnitude analysis of rates of surface diffusion and bulk diffusion

The diffusion of atoms on, or into, a solid lattice, *e.g.* body centred cubic (b.c.c.) Fe, involves diffusing species hopping across the lattice and overcoming energy barriers associated with such a motion on or through the solid phase. The kinetics of this process

follow Fick's Law of diffusion (Cussler, 1997), and the diffusion coefficient, D can be expressed by an Arrhenius equation: $D=D_0\exp(-E/RT)$, where D_0 is a pre-exponential factor, or frequency factor, determined by the properties of the solid lattice (*e.g.* size of the Fe cations) and the diffusing species (Cussler, 1997). The activation energy for diffusion, *i.e.* the energy barrier which the H atom needs to overcome, to move to the next available site, is denoted by E. Consequently, the difference between surface diffusion and bulk diffusion is mainly the difference between the energy barriers for the two processes. It should be noted that the surface energetics are highly dependent on the orientation of the surface (*e.g.* as represented by the Miller "*hkl*" index). For b.c.c iron, most surfaces are (1 0 0) and (1 1 0). Accordingly, the diffusion of surface H atoms into the bulk phase is energetically favoured by the (1 0 0) surface (Jiang and Carter, 2004). Therefore Fe (1 0 0) is the surface of concern in this analysis. Based on the calculation by Sorescu (2005), the energy barriers for an H atom to diffuse to surface sites and into the subsurface sites are 7.9 and 39.7 kJ mol^{-1}, respectively. Therefore the ratio of diffusivities, $D_{surface}/D_{bulk}$ is 30 at 1123 K. Accordingly, the estimated value of $D_{H,bulk}$ by Kiuchi and McLellan (1983), indicates that $D_{surface}=8.4\times10^{-7}\ m^2\ s^{-1}$. The rate of diffusion of oxygen ions through Fe, is calculated using Eq. (30), to be $1.9\times10^{-11}\ m^2\ s^{-1}$, which is more than four orders of magnitude smaller than for H atoms diffusing on the surface of Fe. The rate constant for the initial phase of the reaction, $k_{S,I,H2}=2.6\times10^{-8}\ m^4\ mol^{-1}\ s^{-1}$, calculated from (37), can now be used to calculate the Biot modulus for the initial reaction, using an expression modified from (28): $\beta=2k_{S,I,H2}(1-\varepsilon_0)/(V_{FeO}S_0D_{surface,H})=3\times10^{-4}$. This estimated Biot modulus suggests surface diffusion plays a dominant role in determining the reaction kinetics for $0.05<X<0.2$ for the reduction of wüstite by hydrogen.

References

Barin, I., 1973. Thermochemical Properties of Inorganic Substances. Springer-Verlag, Berlin; New York.

Barrie, P.J., 2011. The mathematical origins of the kinetic compensation effect: 1. the effect of random experimental errors. Phys. Chem. Chem. Phys. 14, 318–326. http://dx.doi.org/10.1039/C1CP22666E.

Benziger, J., Madix, R.J., 1980. The effects of carbon, oxygen, sulfur and potassium adlayers on CO and H_2 adsorption on Fe(100). Surf. Sci 94, 119–153. http://dx.doi.org/10.1016/0039-6028(80)90160-0.

Berger, H.F., Grösslinger, E., Rendulic, K.D., 1992. Coupling of vibrational and translational energy in the adsorption of H_2 on Fe(100): state-resolved sticking coefficients. Surf. Sci. 261, 313–320. http://dx.doi.org/10.1016/0039-6028(92)90242-X.

Bhatia, S.K., Perlmutter, D.D., 1980. A random pore model for fluid-solid reactions: I. Isothermal, kinetic control. AIChE J. 26, 379–386. http://dx.doi.org/10.1002/aic.690260308.

Bhatia, S.K., Perlmutter, D.D., 1981. A random pore model for fluid-solid reactions: II. Diffusion and transport effects. AIChE J. 27, 247–254. http://dx.doi.org/10.1002/aic.690270211.

Bohn, C.D., Cleeton, J.P., Müller, C.R., Davidson, J.F., Hayhurst, A.N., Scott, S.A., Dennis, J.S., 2010. The kinetics of the reduction of iron oxide by carbon monoxide mixed with carbon dioxide. AIChE J. 56, 1016–1029. http://dx.doi.org/10.1002/aic.12084.

Bohn, C.D., Müller, C.R., Cleeton, J.P., Hayhurst, A.N., Davidson, J.F., Scott, S.A., Dennis, J.S., 2008. Production of very pure hydrogen with simultaneous capture of carbon dioxide using the redox reactions of iron oxides in packed beds. Ind. Eng. Chem. Res. 47, 7623–7630. http://dx.doi.org/10.1021/ie800335j.

Chen, W.K., Peterson, N.L., 1975. Effect of the deviation from stoichiometry on cation self-diffusion and isotope effect in wüstite, $Fe_{1-x}O$. J. Phys. Chem. Solids 36 (10), 1097–1103. http://dx.doi.org/10.1016/0022-3697(75)90052-9.

Choudhary, T., Goodman, D., 2002. CO-free fuel processing for fuel cell applications. Catal. Today 77, 65–78. http://dx.doi.org/10.1016/S0920-5861(02)00233-X.

Cleeton, J.P.E., Bohn, C.D., Müller, C.R., Dennis, J.S., Scott, S.A., 2009. Clean hydrogen production and electricity from coal via chemical looping: identifying a suitable operating regime. Int. J. Hydrog. Energy 34, 1–12. http://dx.doi.org/10.1016/j.ijhydene.2008.08.069.

Coombs, P.G., Munir, Z.A., 1990. Investigation of the reduction kinetics of wustite fine powders. Journal of Materials Science 25, 343–352. http://dx.doi.org/10.1007/BF00544229.

Cussler, E.L., 1997. Diffusion: Mass Transfer in Fluid Systems. Cambridge University Press, Cambridge, England.

Davidson, J.F., Harrison, D., 1963. Fluidised Particles. Cambridge University Press, Cambridge, England.

Darton, R.C., La Nauze, R.D., Davidson, J.F., Harrison, D., 1977. Bubble growth due to coalescence in fluidized beds. Trans. Inst. Chem. Eng. 55, 274–280.

Dennis, J.S., Hayhurst, A.N., 1986. A simplified analytical model for the rate of reaction of SO_2 with limestone particles. Chem. Eng. Sci. 41, 25–36. http://dx.doi.org/10.1016/0009-2509(86)85194-6.

Farren, M., Matthew, S.P., Hayes, P.C., 1990. Reduction of solid wustite in $H_2/H_2O/CO/CO_2$ gas mixtures. Metall. Trans. B 21, 135–139. http://dx.doi.org/10.1007/BF02658125.

Geus, J.W., 1986. Preparation and properties of iron oxide and metallic iron catalysts. Appl. Catal. 25 (1–2), 313–333. http://dx.doi.org/10.1016/S0166-9834(00)81249-X.

Giddings, R.A., Gordon, R.S., 1973. Review of oxygen activities and phase boundaries in wustite as determined by electromotive-force and gravimetric methods. J. Am. Ceram. Soc. 56, 111–116. http://dx.doi.org/10.1111/j.1151-2916.1973.tb15423.x.

Green, J.R., Margerison, D., 1978. Statistical treatment of experimental data. Elsevier Scientific Pub. Co.

Green, D.W., Perry, R.H., 2007. Perry's Chemical Engineers' Handbook, eighth ed. McGraw-Hill Professional, New York.

Hayes, P.C., 1979. The kinetics of formation of H_2O and CO_2 during iron oxide reduction. Metall. Trans. B 10, 211–217. http://dx.doi.org/10.1007/BF02652465.

Jiang, D.E., Carter, E.A., 2004. Diffusion of interstitial hydrogen into and through bcc Fe from first principles. Phys. Rev. B 70, 064102. http://dx.doi.org/10.1103/PhysRevB.70.064102.

John, D.H.S., Hayes, P.C., 1982. Microstructural features produced by the reduction of wustite in H_2/H_2O gas mixtures. Metall. Trans. B 13, 117–124. http://dx.doi.org/10.1007/BF02666962.

John, D.H.S., Matthew, S.P., Hayes, P.C., 1984. Establishment of product morphology during the initial stages of wustite reduction. Metall. Trans. B 15, 709–717. http://dx.doi.org/10.1007/BF02657293.

Kierzkowska, A.M., Bohn, C.D., Scott, S.A., Cleeton, J.P., Dennis, J.S., Müller, C.R., 2010. Development of iron oxide carriers for chemical looping combustion using sol–gel. Ind. Eng. Chem. Res. 49, 5383–5391. http://dx.doi.org/10.1021/ie100046f.

Kiuchi, K., McLellan, R.B., 1983. The solubility and diffusivity of hydrogen in well-annealed and deformed iron. Acta Metall. 31, 961–984. http://dx.doi.org/10.1016/0001-6160(83)90192-X.

Li, F., Zeng, L., Velazquez-Vargas, L.G., Yoscovits, Z., Fan, L.-S., 2010. Syngas chemical looping gasification process: bench-scale studies and reactor simulations. AIChE J. 56, 2186–2199. http://dx.doi.org/10.1002/aic.12093.

Li, Z., Sun, H., Cai, N., 2012. Rate equation theory for the carbonation reaction of CaO with CO_2. Energy Fuels 26, 4607–4616. http://dx.doi.org/10.1021/ef300607z.

Liu, W., Dennis, J.S., Scott, S.A., 2012a. The effect of addition of ZrO_2 to Fe_2O_3 for hydrogen production by chemical looping. Ind. Eng. Chem. Res. 51, 16597–16609. http://dx.doi.org/10.1021/ie302626x.

Liu, W., Dennis, J.S., Sultan, D.S., Redfern, S.A.T., Scott, S.A., 2012b. An investigation of the kinetics of CO_2 uptake by a synthetic calcium based sorbent. Chem. Eng. Sci. 69, 644–658. http://dx.doi.org/10.1016/j.ces.2011.11.036.

MATLAB, 2008. MATLAB and Curve Fitting Toolbox Release 2008a. The MathWorks, Inc., Natick, Massachusetts, United States.

Messerschmitt, A., 1910. Process of producing hydrogen. U.S. Patent 971, 216.

Mondal, K., Lorethova, H., Hippo, E., Wiltowski, T., Lalvani, S.B., 2004. Reduction of iron oxide in carbon monoxide atmosphere—reaction controlled kinetics. Fuel Process. Technol. 86, 33–47. http://dx.doi.org/10.1016/j.fuproc.2003.12.009.

Moujahid, S.E., Rist, A., 1988. The nucleation of iron on dense wustite: a morphological study. Metall. Trans. B 19, 787–802. http://dx.doi.org/10.1007/BF02650198.

Reed, H., Berg, H., 1953. Hydrogen process. U.S. Patent 2,635,947.

Ryzhonkov, D.I., Sorin, S.B., 1999. Kinetics of the reduction of wustite of different compositions. Solid State Ionics 117, 145–150. http://dx.doi.org/10.1016/S0167-2738(98)00257-4.

Sorescu, D.C., 2005. First principles calculations of the adsorption and diffusion of hydrogen on Fe(1 0 0) surface and in the bulk. Catal. Today 105, 44–65. http://dx.doi.org/10.1016/j.cattod.2005.04.010.

Sotirchos, S.V., Yu, H.C., 1988. Overlapping grain models for gas-solid reactions with solid product. Ind. Eng. Chem. Res. 27, 836–845. http://dx.doi.org/10.1021/ie00077a020.

Sutherland, W., 1893. LII. The viscosity of gases and molecular force. Philos. Mag. Ser. 5 (36), 507–531. http://dx.doi.org/10.1080/14786449308620508.

Takada, J., Adachi, M., 1986. Determination of diffusion coefficient of oxygen in α-iron from internal oxidation measurements in Fe-Si alloys. J. Mater. Sci. 21 (6), 2133–2137. http://dx.doi.org/10.1007/BF00547959.

Turkdogan, E., Vinters, J., 1972. Gaseous reduction of iron oxides: Part III. Reduction-oxidation of porous and dense iron oxides and iron. Metall. Mater. Trans. B 3, 1561–1574. http://dx.doi.org/10.1007/BF02643047.

Udovic, T.J., Dumesic, J.A., 1984. Adsorptive properties of magnetite surfaces as studied by temperature-programmed desorption: Studies of O_2, NO, CO_2, and CO adsorption. J. Catal. 89, 314–326. http://dx.doi.org/10.1016/0021-9517(84)90308-7.

Van der Laan, G.P., Beenackers, A.A.C.M., 1999. Kinetics and selectivity of the Fischer–Tropsch synthesis: a literature review. Catal. Rev. 41, 255–318. http://dx.doi.org/10.1081/CR-100101170.

Wen, C.Y., Yu, Y.H., 1966. A generalized method for predicting the minimum fluidization velocity. AIChE J. 12 (3), 610–612. http://dx.doi.org/10.1002/aic.690120343.